



# A probabilistic seismic hazard map for the metropolitan France

Stéphane Drouet<sup>1</sup> · Gabriele Ameri<sup>3</sup> · Kristell Le Dortz<sup>3</sup> · Ramon Secanell<sup>1</sup> · Gloria Senfaute<sup>2</sup>

Received: 17 December 2018 / Accepted: 10 January 2020  
© Springer Nature B.V. 2020

## Abstract

This paper presents the development of a probabilistic seismic hazard analysis (PSHA) model to compute seismic hazard maps for the French territory taking into account 15 years of research and development in the area. Since 2002, when the first probabilistic hazard map was computed for France, many new data became available leading to new studies and experience gained. This 2017 PSHA version for France incorporates significant improvements over previous version. In particular, the recent SIGMA project 2010–2016 produced a number of outputs which are used in the present analysis: a homogenized earthquake catalogue in moment magnitude ( $M_w$ ), a Bayesian methodology to compute distributions of maximum magnitudes, ground motion prediction equations specifically developed for the French territory, new seismotectonic analysis conducted based on geological, structural, geophysical, neotectonic and seismological data. Preliminary comparison of median PGA values at 475 years return period with results obtained independently for neighboring countries (Germany, Switzerland, and Italy) reveals a fair agreement. Comparison with the 2013 European Seismic Hazard Model (*ESHM13*, SHARE project) and the model for France developed in 2002 indicates that 2017 PSHA version leads to lower hazard.

**Keywords** PSHA · Hazard maps · France

## 1 Introduction

Probabilistic seismic hazard analysis (PSHA) has become a fundamental tool in assessing seismic hazards. It is used as input for building codes and basis for site-specific evaluation for engineering purposes. In the metropolitan France, the first PSHA map was performed in 2002

---

**Electronic supplementary material** The online version of this article (<https://doi.org/10.1007/s10518-020-00790-7>) contains supplementary material, which is available to authorized users.

---

✉ Stéphane Drouet  
s.drouet@fugro.com

<sup>1</sup> FUGRO France, Auriol, France

<sup>2</sup> EDF R&D, Paris Saclay, France

<sup>3</sup> SEISTER, Aubagne, France

(Martin et al. 2002, hereafter referred to as MEDD2002) giving the bases for the elaboration of the French zoning (<https://www.georisques.gouv.fr/articles>). Later, Marin et al (2004) published PSHA maps for the French territory at returns periods of 475, 975 and 1975 years. In 2013 the European Seismic Hazard Model developed within the SHARE project was published (<https://www.share-eu.org/>). Regarding the application of this last model for areas of moderate seismicity, the scientific community observed an increase of PGA values with respect to the national references.

In the last 15 years the PSHA practice has greatly improved, mainly motivated by several large site-specific projects (e.g. the PEGASOS project), new data became available, the computational codes have been largely improved and research programs have been launched around the world focusing on the consideration and treatment of uncertainties in the PSHA calculations. The accurate evaluation and appropriate treatment of uncertainties is indeed of primary importance particularly in low-to-moderate seismicity regions where the lack of local data needs to be considered and addressed in the development of the hazard model. In this framework, the SIGMA project (Senfaute et al. 2015; Pecker et al. 2017) created a network involving earth scientists, engineers and consultants to better understand the role of the uncertainties in PSHA in order to improve the robustness of the hazard estimates. In order to identify the parameters and uncertainties controlling the seismic hazard estimates and to be able to measure the benefits of the SIGMA research, two applications were performed: one in the Po Plain area in Italy (Faccioli et al. 2015) and another in the South Est region of the French territory (Martin et al. 2017).

The PSHA model developed in the present research account for the outcomes of SIGMA project and complies with the state-of-the-art of regional PSHA in Europe and worldwide. The major improvements integrated in the PSHA model performed in the present study are:

- An homogenous earthquake catalogue with a refined estimates of Mw and depth for historical earthquake that are a major source of uncertainties in the development of the hazard model (FCAT-17, Manchuel et al. 2017);
- The assessment of the maximum earthquake magnitude was defined by applying a Bayesian approach adapted to the French context (Ameri et al. 2015);
- The Seismic Source Characterization (SSC) logic tree was improved by considering recent progress in the PSHA practice and recent scientific publications;
- The set of Ground-Motion Prediction Equations (GMPEs) was selected based on models developed using the ground motion database for the Pan-European region (RESORCE database, Akkar et al. 2014), models specific for France, as well as models based on global datasets to capture epistemic uncertainties in the ground motion scaling in France.

In this paper, the hazard model is developed with the aim of producing a hazard map for 475 years return period and for rock site conditions (i.e.,  $v_{S30}=800$  m/s). The results are compared to those obtained with the most recent hazard models of neighboring countries (e.g., Germany, Switzerland and Italy) as well as with the results of SHARE and MEDD2002.

## 2 Earthquake catalogue

### 2.1 Compilation of the catalogue

A new catalogue for metropolitan France (FCAT-17) has been developed by Manchuel et al. (2017) combining work performed within the framework of the SiHex project (Cara et al. 2015) and SIGMA project (Senfaute et al. 2015; Pecker et al. 2017) on instrumental and historical earthquakes. The historical part of the catalogue relies on the SISFRANCE macroseismic database (<https://www.sisfrance.net/>) for the location of events with re-evaluated moment magnitudes and depth with associated uncertainties (Baumont et al. 2018; Traversa et al. 2017). The instrumental part relies on the SiHex catalogue (Cara et al. 2015, 2017) with a geographical extension limited to a 20 km buffer around the French borders and coastlines. Event location (longitude, latitude and depth) as well as moment magnitude and associated uncertainty are given for all events in the catalogue FCAT-17 which is the backbone catalogue for the current study.

Since our goal is to compute hazard maps for the French metropolitan territory, the catalogue is extended geographically beyond the 20 km buffer used in FCAT-17 by including the events of the SHEEC catalogue (Stucchi et al. 2013) developed within the framework of the SHARE project (Woessner et al. 2015) located outside the French borders. The events of the SiHex catalogue filtered out by the buffer applied to FCAT-17 are also included in the project catalogue, as well as a geographical extension of the SiHex catalogue provided on demand by the authors of SiHex. Finally, in order to include events after 2009, we add the events published in the LDG bulletins ([https://www-dase.cea.fr/evenement/syntheses\\_resultat.php?lang=en](https://www-dase.cea.fr/evenement/syntheses_resultat.php?lang=en)) for the period 2010–2016.

Duplicate events are manually identified for the period pre-1965 where the FCAT-17 and SHEEC catalogues overlap (302 events are removed). Events without any magnitude information in any scale are removed. Finally, only events in the geographical area defined by longitudes between 7°W and 11°E and latitudes between 39°N and 53.5°N are kept.

Table 1 summarizes the characteristics of the project catalogue considering only events with Mw greater than or equal to 2.5 with respect to the different sources, and Fig. 1. presents the repartition of events included in the project catalogue.

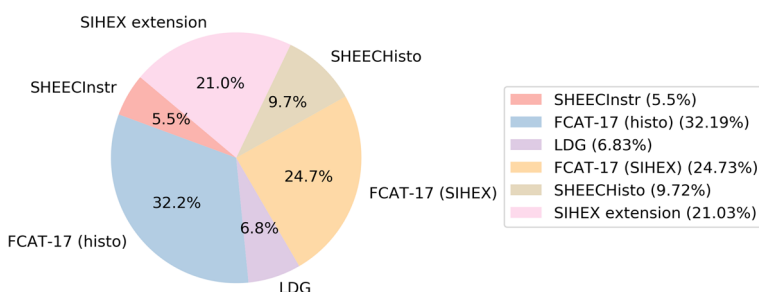


**Fig. 1** Distribution of earthquakes in the project catalogue with respect to the different sources

**Table 1** Main characteristics of the source catalogues (spatial extension: longitudes between 7°W and 11°E; latitudes between 39°N and 53.5°N)

Catalogue	Number of events	Number of events after declustering	Time period	Magnitude range	Hypocentral depth range (km)
FCAT-17 (histo)	3327	2073	463–1964	2.5–6.7 ( $M_w$ )	1–21
FCAT-17 (instru)	2556	1876	1962–2009	2.5–5.2 ( $M_w$ )	0–49
SHEEC (histo)	1005	994	1013–1899	2.5–6.2 ( $M_w$ )	1–20
SHEEC (instru)	568	538	1900–1964	3.5–6.5 ( $M_w$ )	3–29
SiHex extension	2174	1454	1965–2009	2.5–5.6 ( $M_w$ )	0–63
LDG bulletins	706	442	2010–2016	2.9–5.4 ( $M_{L[LDG]}$ )	0–66

## 2.2 Magnitude homogenization

The target homogenized magnitude is the moment magnitude which is consistent with most of the modern GMPEs. All the events already have moment magnitude estimation in the source catalogues except for the LDG events which are characterized by either  $M_L$  or  $M_d$  computed at LDG. We first search for direct estimation of moment magnitudes for these events from moment tensor inversion results from B. Delouis (GeoAzur, Nice, <https://geoazur.oca.eu/spip.php?rubrique59>) and the Swiss Seismological Service (SED, <https://www.seismo.ethz.ch/static/mti/index.html>). We then compared  $M_L$  and  $M_d$  values included in the catalogue and found that one can assume  $M_L = M_d$ . Then we used the same magnitude conversion scheme as proposed in Cara et al. (2015) for the SiHex catalogue:

$$M_w = \begin{cases} 0.45 + 0.664 \times M_{L(LDG)} & \text{if } M_{L(LDG)} < 3.1 \\ M_{L(LDG)} - 0.6 & \text{if } M_{L(LDG)} \geq 3.1 \end{cases}$$

Figure 2 compares the moment magnitudes computed by B. Delouis and the SED with the local LDG magnitudes. The conversion relationship of Cara et al. (2015) is plotted on top. Despite the small number of events with a moment magnitude estimation, the Cara et al. (2015) conversion seems to underestimate moment magnitudes below  $ML[LDG] = 4.0$ –4.5. One has to note that moment magnitudes in the SiHex catalogue are computed from coda wave analysis mostly for events with magnitude  $M_L$  greater than 4.0.

**Fig. 2** Comparison of the moment magnitudes from moment tensor inversion and local LDG magnitudes with the Cara et al. (2015) conversion relationship

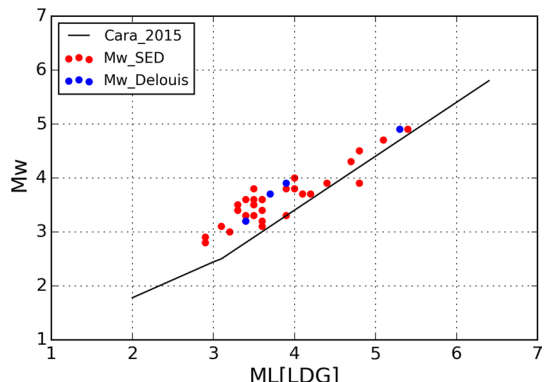
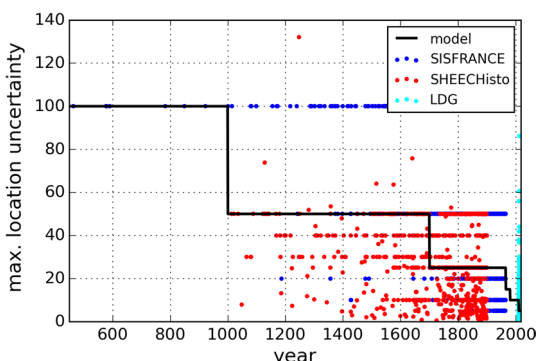


**Table 2** Location uncertainty time-dependent model

Time span	Location uncertainty (km)
Year < 1000	100
1000 ≤ year < 1700	50
1700 ≤ year < 1965	25
1965 ≤ year < 1980	15
1980 ≤ year < 2010	10
2010 ≤ year < 2017	5

**Fig. 3** Location uncertainty from SISFRANCE and the SHEEC and LDG catalogue versus time. The time-dependent model defined in the present study is also shown



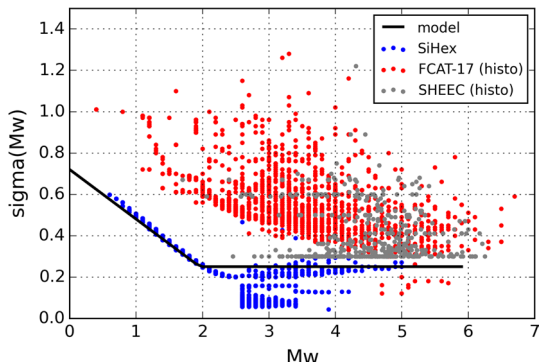
This suggests that further effort is needed to compute moment magnitudes for small events in France which would help to better constrain conversion relationships between magnitude scales. As will be mentioned in the activity rate section magnitude 4.0 is also the point where the instrumental and historical parts of the catalogue overlap and the activity rates coming from both parts may not be fully consistent.

### 2.3 Location and magnitude uncertainties

The FCAT-17 catalogue does not provide location uncertainty. Hypocentral locations are taken from the SISFRANCE database without modifications. Using the location quality index QPOS and associated location uncertainties from SISFRANCE, and the location uncertainties given in the SHEEC and LDG catalogues, we defined a time-dependent model to assign location uncertainty to events without that information. The model is given in Table 2 and Fig. 3 shows the model with the underlying data used to constrain it. Using the time-dependent model gives a first order estimate of the location uncertainty; of course, event specific evaluation, if available, would be a better solution and future improvement of the catalogue should head into that direction.

About half of the events in the project catalogue have moment magnitude uncertainty estimation (events from FCAT-17, SHEEC historical and SiHex catalogues); for the other events (from the SHEEC instrumental, LDG and SiHex extended catalogues) moment magnitude uncertainty must be determined. Figure 4 shows the moment magnitude uncertainty provided in the FCAT-17, SHEEC historical and SiHex catalogues versus moment magnitude. Clearly, moment magnitude uncertainty for historical

**Fig. 4** Moment magnitude uncertainty given in the SiHex, FCAT-17 and SHEEC catalogues versus Mw. The magnitude-dependent model defined in the present study is also shown



events is much larger than that for instrumental events. In both cases, however, there is a tendency of uncertainty decrease with increasing magnitude. Since we are interested to evaluate moment magnitude uncertainty for mainly instrumental events, a magnitude-dependent model is built as shown in Fig. 4.

The compiled catalogue covers the period 463–2016 and includes 10,336 events with magnitudes between 2.5 and 6.7, latitudes between 39°N and 53.5°N and longitudes between 7°W and 11°E. Considering all the events compiled with magnitudes from 0.4 to 6.7, a basic plot of number of events per magnitude bin indicates a minimum completeness magnitude between 1.5 and 2.0. Hypocentral depth for 227 events (~0.3% of the catalogue) are greater than 30 km and have been capped to 30 km in order to remain coherent with the crustal thickness limits used in the PSHA model. We assumed that most probably these are depths not well constrained by the localisation procedure.

## 2.4 Declustering

Most hazard studies rely on a Poissonian model for the modeling of earthquake occurrence implying independence between the earthquakes. Large aftershock sequences, if not removed from the catalogue may bias the estimation of seismic activity rate.

There is no unique solution to separate the time-independent part of seismicity from the seismic activity related to aftershocks, foreshocks or clusters of earthquakes. The most common methods used in hazard studies are those from Gardner and Knopoff (1974) and Reasenberg (1985). These algorithms require a number of input parameters which should ideally tailored to the area under study and/or the catalogue. In the present study, for simplicity, we selected the Gardner and Knopoff (1974) algorithm using the spatio-temporal windows defined by Burkhard and Grünthal (2009) for Central Europe. The impact of using alternative declustering algorithms has not been fully evaluated but preliminary comparisons of activity rates computed using the whole catalogue for magnitudes larger than 3.0 suggested a moderate influence (Table 3).

More than half of the earthquakes in the catalogue are identified as either aftershock or foreshock. Figure 5 shows that the effect of the declustering increases with decreasing magnitude, as expected. Considering only magnitudes above 2.5, out of the 10,336 events, 2959 are identified as dependent events (30%).

**Table 3** Seismic activity parameters (Gutenberg–Richter model a- and b-values) computed for the whole catalogue using two alternatives of the declustering spatio-temporal windows

Spatio-temporal windows	Gutenberg–Richter a-value	Gutenberg–Richter b-value
Burkhard and Grünthal (2009)	$3.62 \pm 0.01$	$0.83 \pm 0.02$
Gardner and Knopoff (1974)	$3.66 \pm 0.01$	$0.84 \pm 0.02$

**Fig. 5** Distribution of moment magnitude in the raw and declustered catalogues

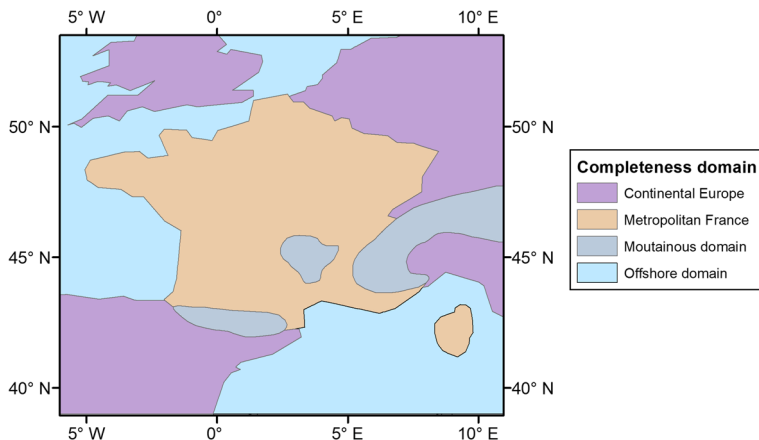
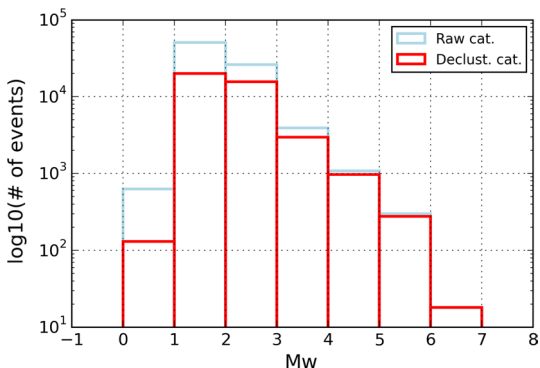


**Fig. 6** Completeness domains

## 2.5 Catalogue completeness with time

Using the compiled project catalogue, we performed a regional completeness analysis separating the offshore regions (Atlantic and Mediterranean), continental France, and mountainous regions (Fig. 6). Intuitively, the potential to detect events in those regions is different. We also included a separate domain for the continental Europe outside France since the final catalogue for these areas is less complete than for continental France, particularly for small magnitudes, because of the backbone catalogues considered in this study.

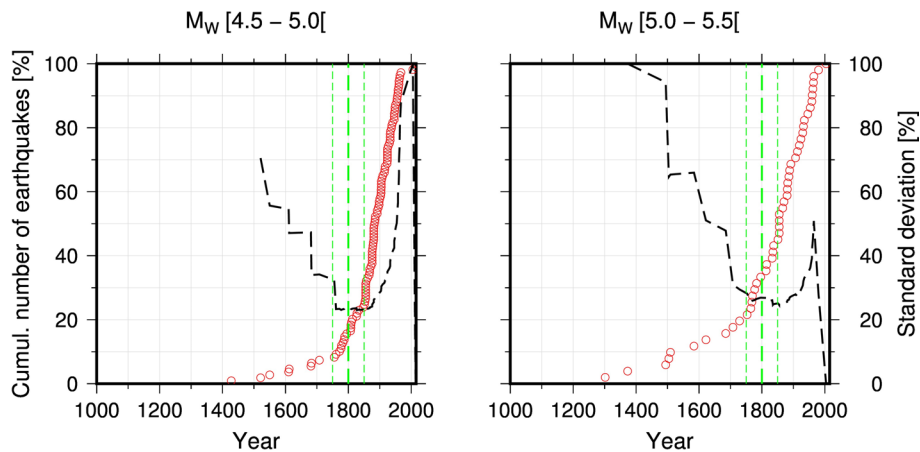


**Fig. 7** Cumulative number of earthquakes versus time (red dots) and inter-event time standard deviation (dashed line) for mountainous domain and 4.5–5.0 magnitude bin (left) and 5.0–5.5 magnitude bin (right). Estimated best-estimate, upper and lower bound of completeness years are also shown (dashed green lines)

**Table 4** Completeness years for each of the 4 completeness domains

Mw bin	Completeness year											
	Continental France			Montainous domain			Oceanic domain			Continental Europe		
	Best	Lower	Upper	Best	Lower	Upper	Best	Lower	Upper	Best	Lower	Upper
[2.5–3.0]	1970	1965	1975	1965	1960	1975	1965	1960	1970	1965	1960	1975
[3.0–3.5]	1950	1940	1960	1965	1955	1975	1965	1960	1970	1965	1960	1975
[3.5–4.0]	1850	1800	1875	1850	1825	1875	1960	1950	1970	1900	1875	1900
[4.0–4.5]	1850	1800	1875	1800	1750	1850	1950	1900	1970	1850	1825	1875
[4.5–5.0]	1700	1650	1800	1800	1750	1850	1800	1700	1850	1800	1700	1850
[5.0–5.5]	1600	1500	1700	1800	1750	1850	1800	1700	1850	1750	1700	1800
[5.5–7.5]	1500	1400	1600	1800	1750	1850	1800	1700	1850	1750	1650	1800

In order to determine the periods of completeness we used the “slope method” based on the cumulative number of events along time, and the Hakimhashemi and Grünthal (2012) method based on the standard deviation of the inter-event time. The analysis is done for each completeness domain and for magnitude bins of 0.5 magnitude unit width. Figure 7 shows an example of computed cumulative number of events and standard deviation of the inter-event time for the mountainous domain and two magnitude bins. We looked for a break of slope in the cumulative number of events, together with a stable standard deviation of the inter-event time. We also imposed an increasing completeness with time. For each magnitude bin we determined a best-estimate completeness year as well as lower and upper bounds (Fig. 7) in order to take into account the level of subjectivity implied by the visual analysis of the plots to determine completeness. The estimated completeness years are given in Table 4 for the 4 completeness domains shown in Fig. 6.

### 3 SSC model

#### 3.1 Area source models

Within regions of moderate seismic activity such as France, seismicity is usually diffuse, and it is difficult to establish a relationship between epicenters and faults. Definition of seismic sources is based on regional subdivisions, covering areas of greater or lesser extent. The objective is to individualize crustal units of homogeneous seismogenic characteristics, following criteria related to static and dynamic state of the seismogenic crust (geometry and kinematic of tectonic structures, distribution of seismic activity, stress field...).

For the construction of our own seismotectonic model (GEOTER), a seismotectonic analysis was conducted based on geological, structural, geophysical, neotectonic and seismological data. This analysis allows the identification of the recent and existing deformation zones related to the current stress field, and to apprehend the deformation mechanisms associated with deep structures. The considered static and structural parameters are: (1) Moho isobaths (e.g., Ziegler and Dèzes 2006), (2) gravimetric and magnetic data (e.g., Martelet et al. 2009), (3), mapping of inherited structures (especially Variscan structures), (4) isopachs maps and Mesozoic sedimentary cover structuration within sedimentary basins, including the location of Triassic salt deposits, and (5) tertiary orogeny tectonic including Pyrenees, Alps and their surroundings.

The identification of seismotectonic units and definition of their boundary generally results from long discussions between specialists and draws from different disciplines to interpret the geological, seismological, geophysical and geodesic measurements and observations. This is why opinions may diverge on the definition of zones or the adoption of one or another model. In order to consider epistemic uncertainties related to the source zones delineation, it is common practice to consider several seismotectonic models in the logic tree. The epistemic uncertainty (i.e. the uncertainty associated with the modelling process) should be adequately assessed, to capture the full range of hypotheses regarding the characterization of the seismic sources and the frequencies of the earthquakes.

In this study, three recent area source models developed at the Metropolitan France scale are considered, which are;

- GEOTER seismotectonic model, which corresponds to our own interpretation of data collected on regional seismotectonic strain mechanisms. This model corresponds to an update of the probabilistic zonation of France (EPAS Zonation, Autran et al. 1998; Bles et al. 1998, Martin et al. 2002). Since 2002, this model has been updated for various GEOTER studies conducted for industrial and nuclear projects by integrating updates of the seismicity catalogue and by taking into account the results of more recent research (international publications, academic research, work of public research agencies: BRGM, IRSN, CEA...). The current model was first developed by defining large seismotectonic units relatively homogeneous at the national scale relying on the analysis of the geodynamic context, on maps of the Moho depth discontinuity (Ziegler and Dèzes 2006), and Bouguer anomaly (e.g., Martelet et al. 2009) to identify the crustal transitional zones (Fig. 8, left). Then, within each large domain a more subtle zoning is performed based on coherent interpretation of available seismological and geological data (Fig. 8, right). The development of the GEOTER model is described in a companion paper (Le Dortz et al. 2019);

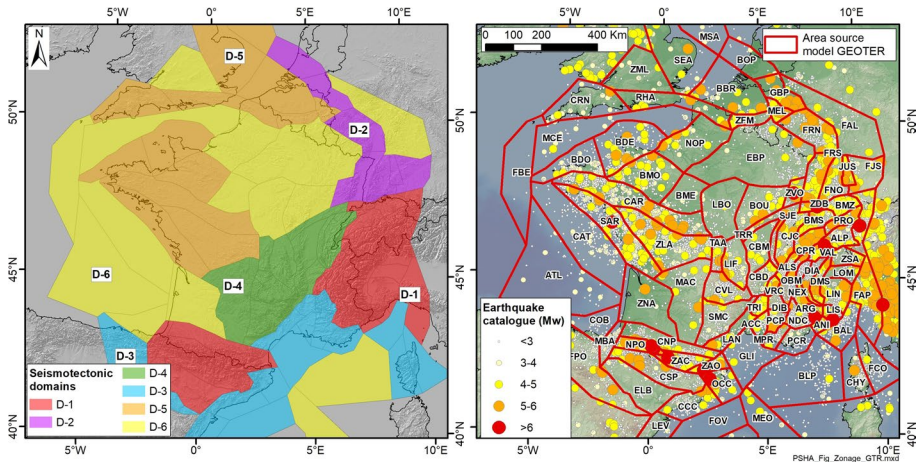
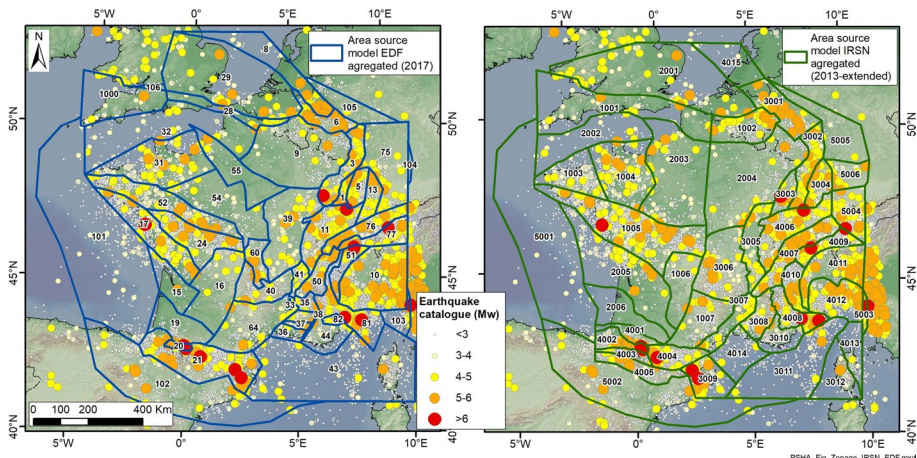


**Fig. 8** Left: large seismotectonic domains. Right: area source model GEOTER

- EDF seismotectonic model (2017), which corresponds to an update of the previous model developed as part of past seismic hazard assessments for nuclear power plants by EDF-TEGG. The development of the model closely follows the regulation guideline for seismic hazard assessment for nuclear installations in France (RFS 2001–01 2001). For the time being no publicly available document exist to describe this model, but a publication is planned by the end of 2019. The georeferenced contours of the new version of the model were made available by EDF (K. Manchuel, pers. Comm.). Within the framework of the probabilistic approach and in agreement with geologist of EDF, we aggregated zones belonging to the same seismotectonic context (Fig. 9, left). Originally developed for deterministic hazard assessment, the EDF source model included very small zones not optimal for PSHA.



- IRSN seismotectonic model, developed by the IRSN (French Institute for Radioprotection and Nuclear Safety) within the framework of its seismic hazard assessment activities and published by Baize et al. (2013). This model is derived from the deterministic zonation published by Berge-Thierry et al. (2004) and takes into account the most recent data regarding deep and shallow geology, as well as those related to tectonic and seismotectonic activity. The IRSN also provides an aggregated version of the seismotectonic model covering larger zones to gather enough data that is more appropriate for probabilistic approach and which is used for this study (Fig. 9, right).

For France and border regions, these alternative models reflect the geodynamic diversity of the NW part of the European platform characterised by differentiated intraplate deformations, between the Orogenic domains (Alpes, Pyrenees), the rifting zone (Rhine graben, Limagnes), the domains with strong Variscan structural inheritance (e.g., Armorican massif), and the stable domains (Parisian basin, Aquitaine basin). Besides, in order to cover the 200 km radius around the French border and coast needed for the elaboration of hazard maps, some “closure zones” were added to the original EDF and IRSN models.

### 3.2 Maximum magnitude

The maximum magnitude assumed to be possible in a region ( $M_{\max}$ ) is an important parameter for seismic hazard studies, although its impact becomes significative only when relatively low annual probabilities of exceedance and/or low frequencies are considered.

In stable continental regions or regions with moderate seismicity the Bayesian method originally developed by Johnston et al. (1994) and updated in EPRI (2012) has become the current practice. A prior distribution is computed from a large region with similar tectonic context as the region under interest which is subsequently updated using a Bayesian approach relying on the observed catalogue in the region of interest. The likelihood function used to update the prior distribution has the following formulation:

$$L(M_{\max}) = \begin{cases} 0 & \text{for } M_{\max} < M_{\max\_obs} \\ [1 - \exp(-b \ln(10)(M_{\max} - M_0))]^{-N} & \text{for } M_{\max} \geq M_{\max\_obs} \end{cases}$$

where  $M_{\max\_obs}$  is the maximum observed magnitude in the target zone,  $b$  is the b-value,  $M_0$  is a given magnitude threshold, and  $N$  the number of events with magnitude greater than or equal to  $M_0$  in the target zone.

The Bayesian approach has been applied in national PSHA in Europe (e.g., Grünthal et al. 2018; Wiemer et al. 2016) by adapting the Johnston et al. (1994) to the target regions. In our application of the Bayesian approach, we use the prior  $M_{\max}$  distributions have been determined by Ameri et al. (2015) for use in low and moderate seismicity regions in France. Ameri et al. (2015) defined two priors: one for active regions including the Alps, the Pyrenees, most of Italy, and Eastern Europe excluding Albania, Greece and Bulgaria; one for stable and low-seismicity regions including the north-western European platform. The parameters for these two  $M_{\max}$  Gaussian distributions are  $\mu=6.8$  and  $\sigma=0.4$  for the active regions, and  $\mu=6.2$  and  $\sigma=0.5$  for the stable regions. These priors are then updated based on the likelihood function defined above using information within the project catalogue.

We applied a truncation on the prior  $M_{\max}$  distribution at a lower bound as well as at an upper bound (Table 5). The  $M_{\max}$  prior distributions are represented by unbounded normal distributions; however, there is likely an upper limit to the size of earthquakes that can

**Table 5** Parameters for the Mmax likelihood function for the 6 large seismotectonic domains

Domain	Prior Mmax distribution	Lower truncation	Upper truncation	$N_{eq}(M \geq M_0 = 4.5)^a$	$M_{max\_obs}^b$	b-Value
D-1	Ameri et al. (2015) active	5.5	7.5	149	6.7	0.79
D-2	Ameri et al. (2015) stable	5.5	7.1	42	6.3	0.78
D-3	Ameri et al. (2015) stable	5.5	7.1	24	6.1	0.87
D-4	Ameri et al. (2015) stable	5.5	7.1	21	5.9	0.89
D-5	Ameri et al. (2015) stable	5.5	7.1	67	6.3	0.96
D-6	Ameri et al. (2015) stable	5.5	7.1	12	5.7	1.01

<sup>a</sup>Number of events within the completeness period with magnitude greater or equal to  $M_0$

<sup>b</sup>Maximum observed magnitude

occur in France. A lower bound is also applied on the prior Mmax distributions because we consider that we do not have the appropriate data and geological arguments to exclude the occurrence of magnitude below Mw 5.5.

For the active domain D-1 (see Fig. 8), we computed a maximum magnitude upper bound of 7.3 based on scaling relationship (Wells and Coppersmith 1994; Papazachos et al. 2004; Wesnousky 2008), considering a maximum rupture length of 60 to 100 km. However, Wiemer et al. (2009) suggest Mmax as high as 7.5 for Switzerland which is finally used for domain D-1. For the Rhine Graben (D-2), our estimate based on maximum rupture length leads to  $M_{max} = 7.0$  and paleoseismological studies suggest maximum magnitudes ranging from 6.3 to 7.1 (Camelbeeck et al. 2000; Vanneste and Verbeek 2001; Vanneste et al. 2013). For domain D-2 the upper bound Mmax is set to 7.1, as well as for all the other domains in the absence of additional data. Note that these values are adapted to a large-scale study and the short return periods of interest targeted in the present study. For site-specific seismic hazard a more detailed analysis of the region of interest may lead to another logic tree for the Mmax. We also performed a sensitivity analysis on the Mmax model using different priors, and the Mmax values from the ESHM13 (Woessner et al. 2015) and estimated an impact lower than 10% on the hazard results. Hence, a single Mmax model is used for the final computation.

The parameters used for the 6 seismotectonic domains are given in Table 5 and the prior and updated (posterior) Mmax distributions are shown in Fig. 10. The method used to determine the b-values given in Table 5 is presented in the next section.

### 3.3 Hypocentral depth distribution

The impact of hypocentral depth of the earthquake on the ground-motion amplitude is usually taken into account through the definition of the distance between the site of interest and the source (e.g. distance metric which takes into account hypocentral depth).

We performed an analysis of the depth distributions within each activity domains using the earthquake catalogue developed for the study. The distributions including all the magnitudes and only events with magnitude greater than 4.5 (the minimum magnitude used for PSHA computation) are compared, and statistics based on the large magnitudes sample are computed (Table 6). Despite the large uncertainties associated to hypocentral depth estimation, the data seems to indicate that hypocentral depths tend to be slightly shallower in

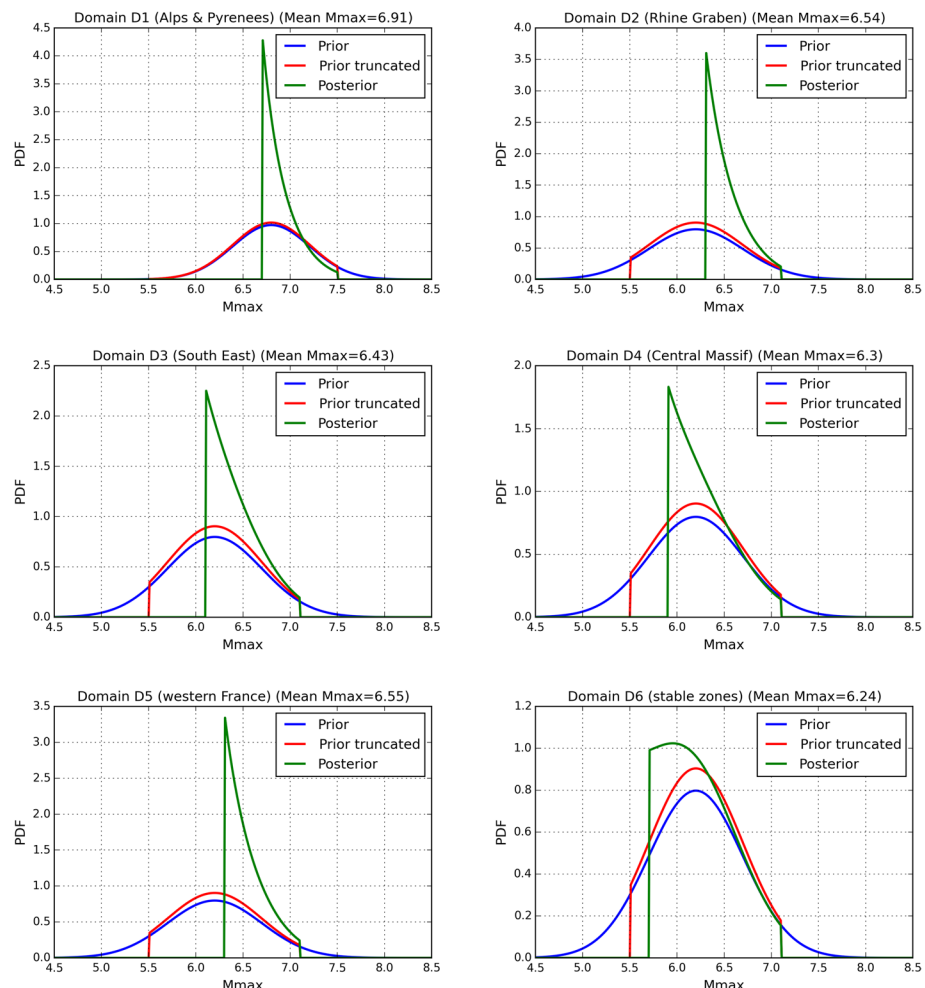


**Fig. 10** Prior and posterior (after Bayesian update) Mmax distributions for the 6 seismotectonic domains

domains D-1 to D-4 compared to domains D-5 and D-6 (western part of France and stable domain).

For comparison, Manchuel et al. (2017) performed an analysis of hypocentral depth distribution considering different regions in France. This work is based on the estimation of moment magnitude and hypocentral depth based on macroseismic intensities. They also find deeper depths in the western part of France (Atlantic and Armorican Massif), and also identified areas with specific characteristics (Hainault, Tricastin, Provence) characterized by shallow depth distribution.

Based on the statistical analysis of depth distribution deduced from the earthquake catalogue and using the geological information such as geometry of crustal structures inferred from the interpretation of deep seismic profiles, the depth ranges retained for each domain are expressed between two limits [Hmin and Hmax] to take into account the uncertainties of this parameter and the natural variability in focal depths of earthquakes in the crust

**Table 6** Hypocentral depth statistics for the large domains for  $Mw \geq 4.5$ 

Domain	Hypocentral depth (km)				
	5th percentile	16th percentile	50th percentile	84th percentile	95th percentile
D-1	5	7	10	15	17
D-2	2	6	11	12	19
D-3	4	5	10	13	19
D-4	9	11	12	15	18
D-5	10	12	14	17	20
D-6	8	11	14	20	20

(Table 7). Table 7 also highlights subdivisions of the large domains in order to take into account hypocentral depth specificities of a number of regions.

Note that these depth limits are related to hypocentral depth only whereas fault ruptures can extend shallower (reaching the surface) and deeper according to seismogenic layer defined between 0.1 and 30 km.

In the SIGMA PSHA (Martin et al. 2017) as well as in the PEGASOS Refinement Project (<https://www.swissnuclear.ch/de/downloads.html>), magnitude-dependent depth distributions have been used. In the present study no clear variation of hypocentral depth with magnitude is observed and the distributions for large events ( $M \geq 4-4.5$ ) may be relatively well modelled using a simple centred triangular shape which is used in the hazard calculation. Hypocentral depth distribution is directly accounted for in the hazard integral since it is an aleatory uncertainty.

### 3.4 Deformation mechanisms

For each zone of each area source model, the deformation mechanism is expressed in terms of percentages of strike-slip, reverse and normal faulting.

For the GEOTER model, a database of focal mechanisms and in-situ stress measurements was compiled from the available sources (scientific publications, reports, online catalogues...). For the seismic zones where sufficient data were available, a prevailing

**Table 7** Depth range retained for zones within each large activity domain

Domain	Zones covering regions of	Retained range depth (km)
D-1	Alps	3–17
	Pyrenees	5–15
D-2	All	5–20
	Provence and BAL	3–8
D-3	Others	3–20
	Jura	3–15
D-4	Others	5–20
	All	5–25
D-5	All	5–20

deformation mechanism was determined based on a calculation of regional stress tensors. When data were insufficient to calculate a correct stress tensor, similar zones were grouped. The tensors were calculated through inversion of focal mechanism data and insitu stress data using the TENSOR software (Delvaux 1993; Delvaux and Sperner 2003).

For EDF model, the dominant deformation mechanism was defined independently by EDF geologists according their own interpretation of geological and seismological data.

For the IRSN model, the dominant deformation mechanisms associated with zones of are mainly inspired by the seismotectonic map of France (Grellet et al. 1993) and by the World stress map from (Heidbach et al. 2009; Baize et al. 2013).

### 3.5 Activity rates

The computation of seismic activity rates is based on the Gutenberg–Richter model which can be written as:

$$N = 10^{a-b \times M}$$

where N is the annual number of events with magnitude larger than or equal to M. Or in its truncated form:

$$N = 10^a \frac{e^{-b \times \ln(10) \times M} - e^{-b \times \ln(10) \times M_{max}}}{1 - e^{-b \times \ln(10) \times M_{max}}}$$

The method used to determine the coefficients a and b of the model is based on the EPRI (2012) method which is an updated and improved version of the Weichert (1980) method. In particular, it allows:

- The consideration of non-uniform magnitude bins;
- The use of regionally varying completeness periods;
- The introduction of a prior on the slope of the GR model (b-value);
- The propagation of uncertainties on earthquake location, magnitude and completeness periods through the use of synthetic catalogues.

Starting from the project catalogue, synthetic catalogues are computed using Gaussian distributions to propagate the uncertainty for location and magnitude. The Gaussians are truncated at 3 sigma's for magnitude and 1 sigma for location uncertainty in order to avoid events occurring hundreds of kilometers away from their original locations. Moreover, uncertainties on completeness years are also propagated for the calculation of the activity rates adopting a uniform distribution.

The regional completeness is accounted for directly in the calculation. Each zone of the seismotectonic models can overlap with multiple zones of completeness, in which case the observed activity rates are computed counting the number of events in each sub-zone and taking into account to corresponding completeness periods.

The fit is performed if at least two magnitude bins are populated (implying at least 2 events with different magnitudes). Otherwise, the b-value is fixed at the prior value and only the a-value is estimated.

The GR models are computed in two-steps. First, we estimate a model for each of the six large domains defined at national level (Fig. 8, left), using a prior on the b-value equal to 1.0. These models are based on large catalogues (i.e. the domains cover wide geographical areas) and we expect stable estimates of the Gutenberg–Richter models. The computed

b-values for the 6 domains are reported in Table 5. Then, in a second step, GR models are computed for each area source using a prior b-value equal to the b-value of the domain to which the zone belongs. The correlation between a and b is also computed and is used for the propagation of uncertainty on the seismic activity parameters. Figure 11 shows an example of GR fit to the domain D-6 and Fig. 12 an example for the zone ACC of the GEOTER model where only few events are available.

The GR modeling results using the maximum likelihood method strongly depend on the activity rates computed for the lower magnitude bins considered. Hence the selection of the minimum magnitude for the fit is a crucial step. After tests using different values between 2.0 (the estimated minimum completeness magnitude for the catalogue) and 4.0, a minimum magnitude between 3.0 and 4.0 is selected depending on the domain or zone. As discussed in the catalogue section, the magnitude homogenization

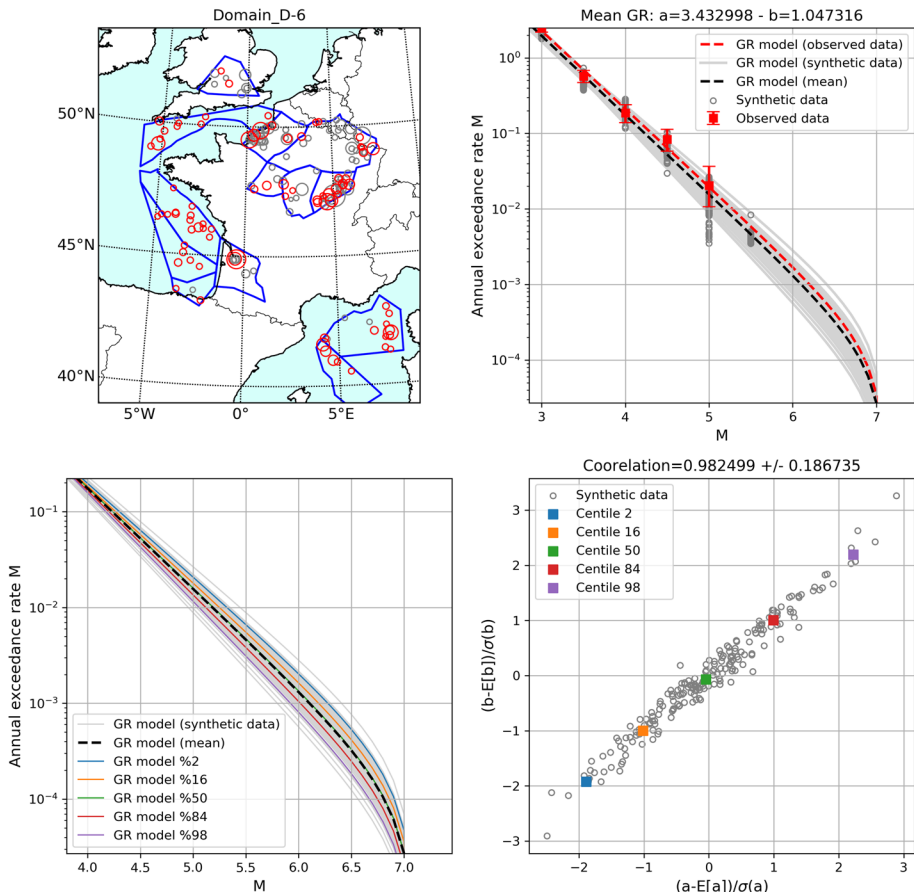


**Fig. 11** Summary of the GR fit to domain D-6. Top left: map of the earthquakes located within the domain (within completeness: red circles; not in the completeness: grey circles). Top right: observed and synthetic annual exceedance rates (red squares and dark gray circles) with GR fit to observed and synthetic data (dashed red and grey lines) and mean GR fit from synthetic data (dashed black line). Bottom left: GR fit to synthetic data (grey lines) with associated statistics. Bottom right: correlation between a and b (normalized residuals are plotted) with associated statistics

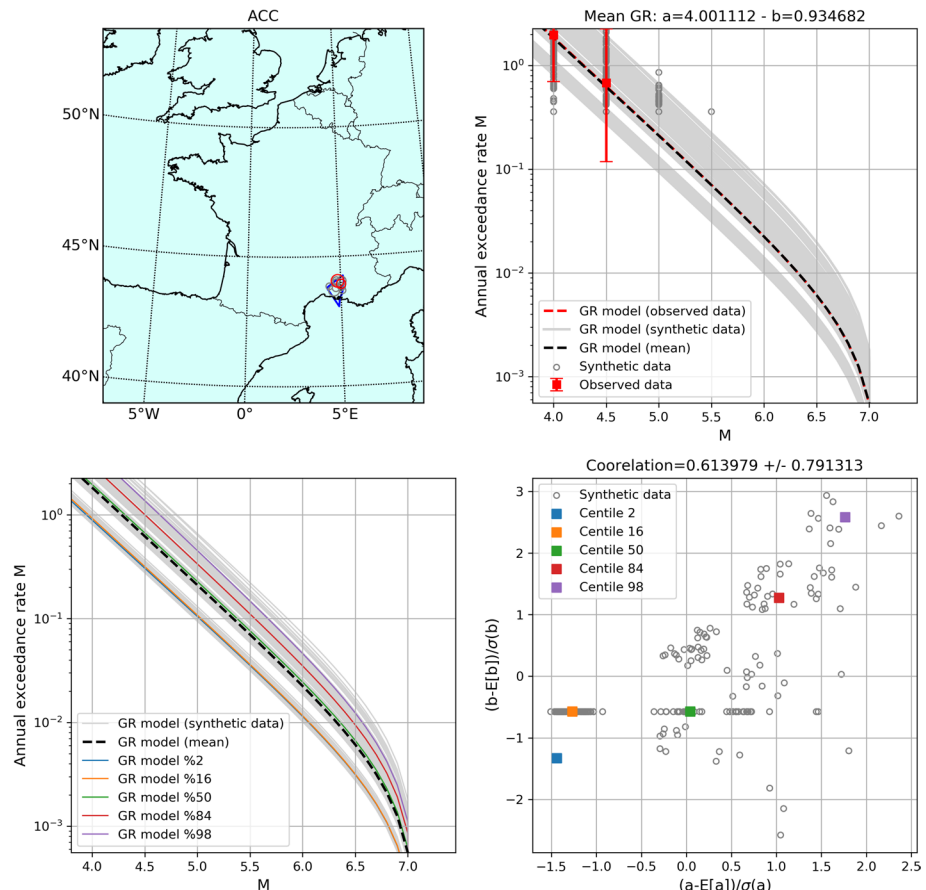


**Fig. 12** Same as Fig. 11 for zone ACC of the GEOTER source model where only few events are included

is less reliable for magnitudes below 4.0. In addition, when the GR modeling led to incoherent values ( $b$ -value outside the 0.7–1.3 range), aggregation of zones was performed. The aggregation was performed between zones belonging to the same tectonic domain and with a common boundary. About 40% of the zones were included in an aggregation for the IRSN model, 50% for the GTR model and 36% for the EDF model.

Note that magnitude uncertainty can lead to bias in the estimation of the activity rates (Tinti and Mulargia 1985; EPRI 2012). Tinti and Mulargia (1985) and EPRI (2012) proposed corrections of this bias based on adjustment of the computed recurrence rate by the exponential of the variance. The Tinti and Mulargia (1985) approach considers a constant magnitude uncertainty while the EPRI (2012) allows taking into account the specific uncertainty for each event of the catalog. EPRI (2012) also recognizes that an additional source of bias may arise from conversions from intensity or other magnitude scales which may act in the opposite way limiting the need for the bias correction. To solve this issue properly and apply a robust and appropriate correction to the computed activity rates, the original direct magnitude estimation and the conversion scheme as well as associated uncertainties applied for each magnitude entry in the catalogue must

be known. In the present study, no correction is applied but his aspect would be further investigated in future updates.

The GR parameters for all the zones or groups of zone (when aggregation was necessary) of the three seismotectonic models are provided as Electronic Supplement to this paper.

### 3.6 Zoneless model

As an alternative to the area source models, the zoneless approach can be used to model seismic activity in the region of interest (e.g., Woessner et al. 2015; Petersen et al. 2018). The method relies on the seismic catalogue and on the large seismotectonic domains defined previously (Fig. 8, left). For each event, a kernel function is used, which is a kind of spatial probability density function, and the summation of these kernels allows us to estimate the activity rates for a grid of points (Woo 1996; Helmstetter and Werner 2012).

A preliminary sensitivity analysis was carried on in order to test two algorithms to build the kernel functions: one called “adaptive” which uses the distance to a given number of closest events to define the kernel (similar to Helmstetter and Werner 2012), and another called “fixed” which defines a fixed kernel, the shape of which depends on magnitude only (similar to Woo 1996). In both cases, the kernels shape is conditioned through a parameter (number of closest events for the adaptive kernels or width of the kernel for the fixed ones) which determines the level of smoothing applied to the observed seismicity. Extremely high parameters would lead to almost uniform activity rates over the domain of interest. The minimum magnitude used to compute the kernels also has an impact on the results.

The activity rates are estimated using a penalized maximum likelihood method using prior b-values equal to those computed for the large seismotectonic domains (see Table 5) and taking into account the regional completeness periods. The Mmax values defined for the large seismotectonic domains are used to construct a truncated GR model for each grid point. Strict boundary conditions are imposed meaning that the kernels cannot cross the domains boundaries.

A sensitivity analysis has been performed in order to evaluate the impact of the kernel type, its parameterization as well as the minimum magnitude selected ( $Mw = 2$  and 3 have been tested) on the estimation of the seismic activity rates and the impact assessed on the resulting seismic hazard results. Overall the variability introduced is low which led us to use a single smoothed seismicity model for the PSHA computations. The selected model is the adaptive kernel using the 10 closest neighbors with a minimum magnitude of 3.0 consistent with the range of minimum magnitudes used for the GR fit for the area source models. The map of the computed a-value using this model is shown on Fig. 13, together with a map of the number of events with magnitude  $Mw \geq 6$  predicted by this model. The maps highlight the high seismic activity in the Alps and the Pyrenees, as well as moderate activity in the Rhine Graben and in Western France.

The computed seismic activity rates for two sites, Brest and Nice are compared on Fig. 14 (the location of these two sites is shown in Fig. 13). Seismic activity rates for the zones hosting the site in the area source models are shown as well as for points in the smoothed seismicity grid located within 20 km of the site. Note that the rates are normalized to an area of  $1e6 \text{ km}^2$  and are consequently directly comparable. For Brest, the results are relatively close while for Nice a large variability is observed. Figure 15 compares the area source models and the smoothed seismicity model for Nice. This figure shows that Nice lies in a transition zone between high seismic activity to the East and lower activity to the West which implies large

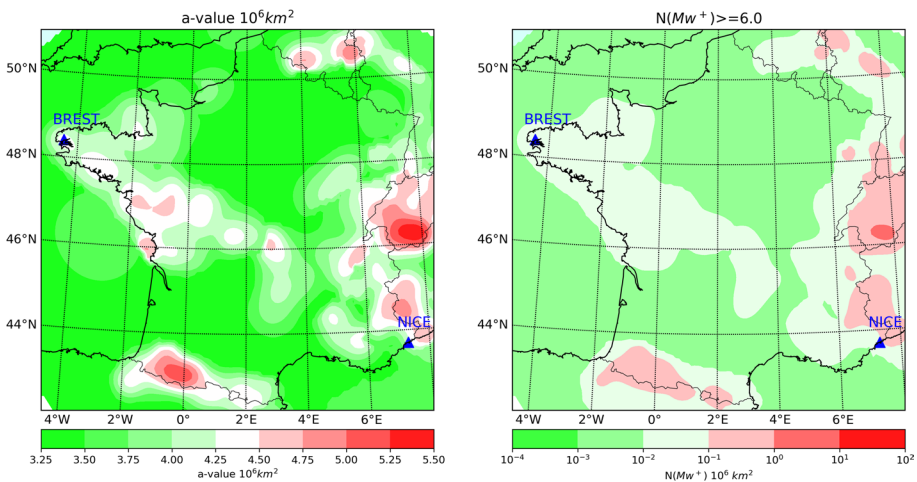


**Fig. 13** Map of the a-values computed using the smoothed seismicity model (left) and of the number of earthquakes with magnitude  $Mw \geq 6$  (right)

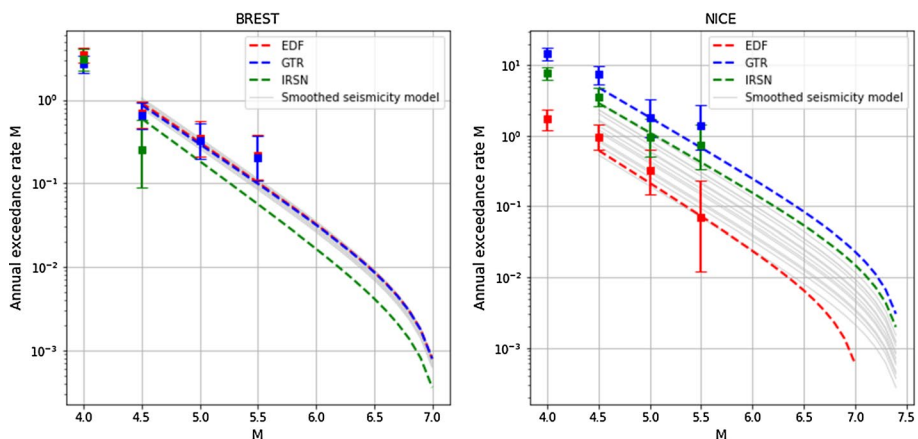


**Fig. 14** Comparison of observed (squares) and modelled (lines) activity rates using the three seismotectonic models and the smoothed seismicity model (all the points of the grid located within 20 km of the site are considered; grey lines) for Brest (left) and Nice (right)

uncertainty in the predicted seismic activity rates depending on the delineation of the area source model. A similar variability range is observed between the activity rates for points of the smoothed seismicity model located within 20 km of the site.

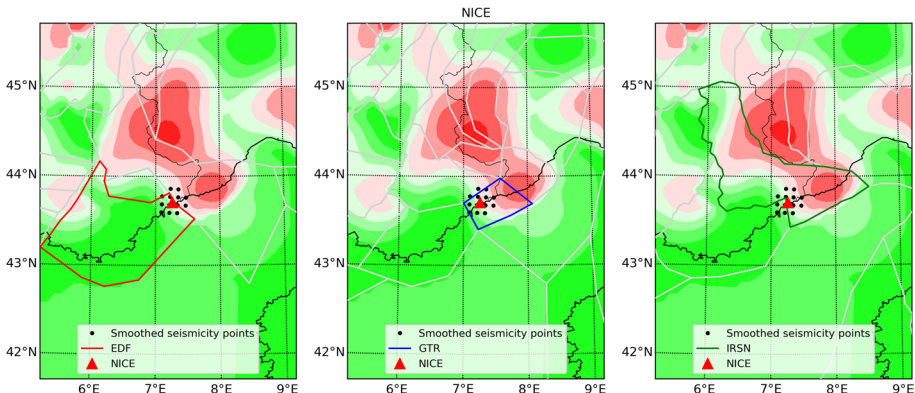


**Fig. 15** Maps of the three area source models (EDF: left; GTR: middle; IRSN: left) with the zone of the site highlighted in color superimposed on the smoothed seismicity a-value map for site Nice (red triangle). Location of the smoothed seismicity grid points within 20 km of the site are depicted as black circles

## 4 Ground-motion characterization model

### 4.1 Selection of GMPEs

The characterization of the ground motion in metropolitan France is clearly a major challenge. Metropolitan France is characterized by a low-to-moderate seismicity and consequently the available strong-motion records are very limited in the magnitude/distance range of interest for seismic hazard assessment. As a result, seismic hazard assessment in France is typically performed using GMPEs derived from data collected in other regions. A common approach to build a Ground-Motion Characterization (GMC) model for PSHA (see Delavaud et al. 2012) consists in several steps:

- Pre-selection of GMPEs applicable for the target seismotectonic context;
- Critical review of the selected GMPEs through objective criteria (validity range of the modeling parameters, compatibility with the requirements of the PSHA calculation...);
- Comparison with observed strong-ground motions and ranking based on the results.

In this study, we made the assumption that GMPEs for active regions are the most relevant for the French context. The target site conditions are set to  $v_{S30}=800$  m/s since the goal of the study is to produce hazard maps for standard rock conditions. We note, however, that in the SHARE project (Woessner et al. 2015) a mixture of GMPEs for active and stable regions have been used for central and western France. This approach would require adjustments between GMPEs especially in terms of site condition characteristics (GMPEs for SCR are typically valid for very hard rock sites). Such adjustments carry large uncertainty which would lead to an increase of the GMPEs standard deviations. Moreover, most of the GMPEs for SCR regions are developed for Eastern US which is characterized by peculiar attenuation of ground-motion with distance (Bakun and McGarr 2002) and their application to the French context is questionable.

Beauval et al. (2012) tested a number of these GMPEs against French strong-motion records and found that the best-fitting models over the whole frequency range are the Cauzzi and Faccioli (2008), Akkar and Bommer (2010), and Abrahamson and Silva (2008)

models. However, these models are now superseded by more recent versions based on updated and augmented databases and functional forms.

Within the SIGMA project, a major outcome was the release of the RESORCE database (<https://www.resorce-portal.eu/>) that contains records for the Pan-European region, aiming at the testing and development of new GMPEs. Based on RESORCE, several new models have been produced (see Douglas et al. 2014a, b). However, although being based on European data these GMPEs do not consider French records in their datasets. For this reason, two GMPEs have been developed focusing on the use of French data: the empirical model by Ameri (2014) and the stochastic model by Drouet and Cotton (2015) (erratum published in Drouet 2017). Note that the model by Ameri (2014), available as a SIGMA project report, has been later improved and published by Ameri et al. (2017). Nevertheless, the two models are similar and the main differences concern the stress parameter model which is not used in the present study, and the sigma model for which the impact in the final results can be considered minor.

The pre-selected models in the present study include the Pan-European models based on RESORCE, the NGA-West2 set of GMPEs (Bozorgnia et al. 2014) as well as the Cauzzi et al. (2015) and Drouet and Cotton (2015) GMPEs. Based on the testing results by Beauval et al. (2012) and on our own critical review of the GMPEs, the final set of GMPEs is:

- Ameri et al. (2017) (generic no stress parameter/RJB)
- Abrahamson et al. (2014)
- Cauzzi et al. (2015) (variable reference  $v_{S30}$  option)
- Drouet and Cotton (2015) (RRUP, 10 MPa stress drop for large events)

## 4.2 Evaluation of the GMC model

The goal of the GMC logic tree is to capture the center, body and range of the technically defensible interpretations of ground motion models, representing the epistemic uncertainties in the GMC for the target site. Ideally these models would be mutually exclusive and collectively exhaustive. The challenge in building such a GMC logic tree is that many GMPEs could be proposed, but we are not sure that the selected models sample the ground-motion space adequately. For example, there may be redundant models; i.e., GMPEs that provide similar ground motions because they are based on the same data and models. These models artificially reduce the epistemic uncertainties. On the other hand, there may be missing models; i.e., models that are missing simply because we have not yet observed certain types of ground motions. In this framework, it is important to visualize the ground motions space that we would like our GMPEs set to cover.

We used several tools in order to explore the proximity of the selected GMPEs with respect to the full set of pre-selected GMPEs. We first draw trellis plots to visualize the differences in distance and magnitude scaling, in spectral shapes and standard deviations. Figure 16 compares the predicted response spectra by the set of pre-selected GMPEs and ones finally included in the GMC model for magnitude-distance scenario that usually contribute more to the hazard in regions of low to moderate seismicity (i.e.  $Mw = 4.5, 5.5$  and  $6.5$  and epicentral distance  $REPI = 1, 10$  and  $50$  km). Figure 17 shows a similar comparison for the standard deviations of the GMPEs.

We also created Sammon's maps (see Scherbaum et al. 2010 for application of Sammon's maps to GMPEs visualization) which allow a visual comparison of ground-motions from various combinations of predictive parameters ( $M, R, \dots$ ) in single plots. Figure 18

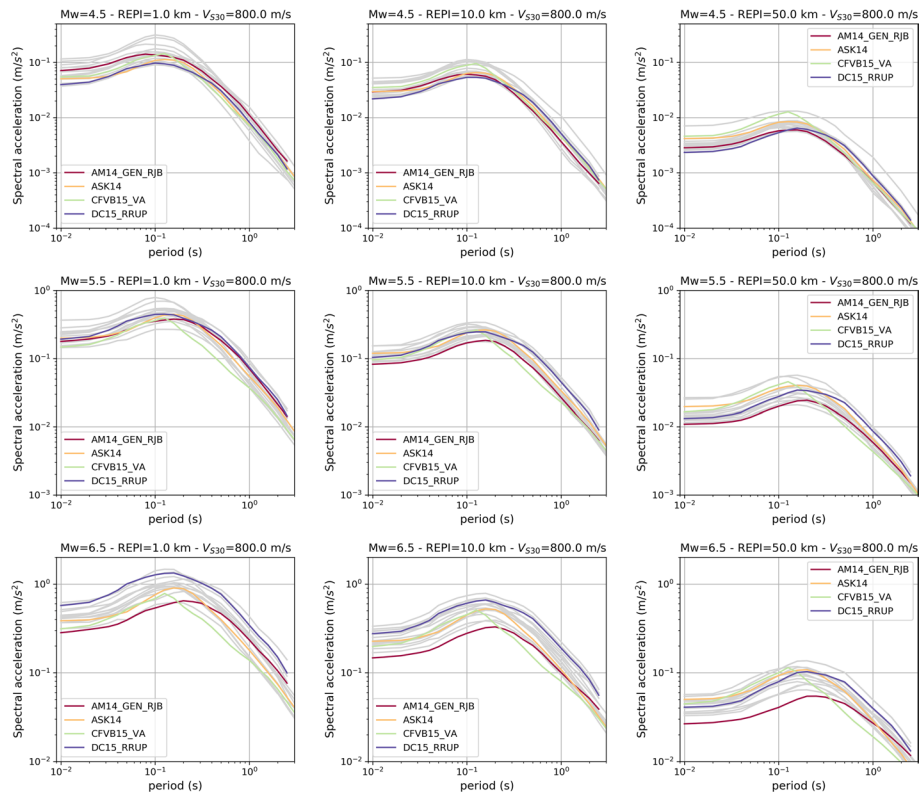


**Fig. 16** Trellis plot of spectral acceleration versus period for 3 magnitudes (top: 4.5; middle: 5.5; bottom: 6.5) and 3 distances (left: 1 km; center: 10 km; right: 50 km). Colored lines present the GMPEs included in the GMC model and grey lines shown the set of pre-selected GMPEs

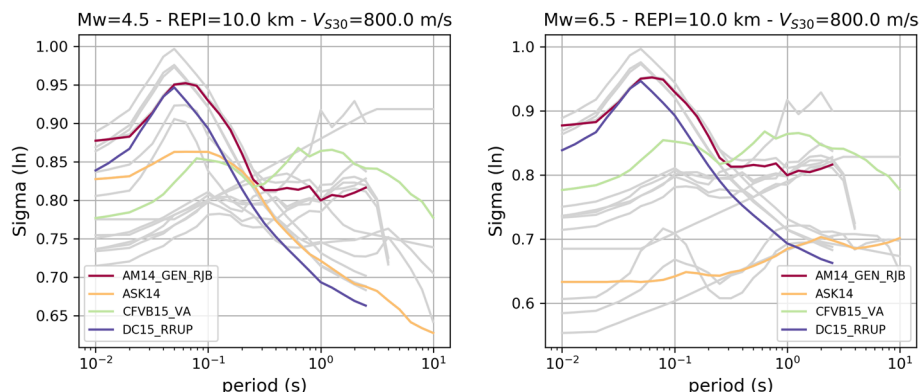
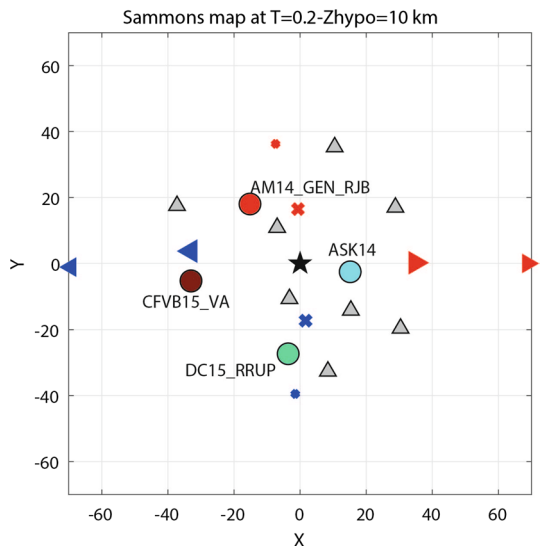


**Fig. 17** Trellis plot of GMPE standard deviation (sigma) versus period for 2 magnitudes (left: 4.5; right: 6.5) and for 10 km epicentral distance. Colored lines present the GMPEs included in the GMC model and grey lines shown the set of pre-selected GMPEs

**Fig. 18** Sammon's map for 0.2 s spectral periods. Ground-motions predicted by the different GMPEs (grey triangles: all pre-selected GMPEs; colored circles: GMPEs selected for PSHA) have been computed for magnitudes between 4.5 and 5.5 and distances between 1 and 50 km (which are the scenarios that most contribute to hazard in low-to-moderate seismicity regions) and  $v_{S30} = 800$  m/s. The black star represents the mean of all the GMPEs. The red and blue triangles represent the mean of all GMPEs scaled by 0.6, 0.8, 1.3, 1.6 respectively. Crosses denote models with faster (red) or slower (blue) attenuation with distance than the mean of all the GMPEs



presents an example of Sammon's map for 0.2 s spectral period showing that the selected GMPEs cover a large portion of the space delimited by the full set of pre-selected GMPEs.

In addition, we also computed the hazard for a single SSC model using the selected GMPEs and the full set of GMPEs and compared the mean, maximum and minimum uniform hazard spectra (UHS) for both GMC models. All these tests allowed us to assess that the selected GMC model reasonably covers the center, body and range of the ground-motion distribution predicted by the full set of pre-selected GMPEs.

## 5 Logic-tree

The logic-tree used to compute PSHA includes 2 types of source models: three area sources and one zoneless model. The zoneless model is assigned a weight equal to 1/3, since at the target short return period of 475 years it is likely a good representation of future seismic sources distribution; however, we did not use a higher weight in order to have a balance between the smoothed seismicity model and the area source models. The remaining 2/3 are equally distributed between the 3 area source models. The four GMPEs are equally weighted in the absence of comparison with observed strong-motion data which could help to define the weights (Delavaud et al. 2012).

We also explored aleatory uncertainty related to hypocentral depth distribution and virtual fault orientation. A triangular distribution is used for hypocentral depth between two bounds (see Table 7). Virtual faults are used to compute the various distance metrics for the GMPEs. For each zone, the PSHA software allows us to define fault orientation for the three main mechanisms (normal, reverse and strike-slip) and assign a probability to each of the mechanisms. For all the cases fault strike can vary between 0° and 360° but fault dip depends on the mechanism. It can vary between 80° and 90° for strike-slip faulting, 50° and 70° for normal faulting and between 30° and 60° for reverse faulting.

In addition, epistemic uncertainty on the seismic activity parameters and maximum magnitude is also propagated using Monte-Carlo sampling (100 samples). Gaussian

distributions truncated at 3 sigmas are used for the seismic activity parameters, taking into account the correlation between  $a$  and  $b$ , and the  $M_{max}$  distributions computed with the Bayesian method are used (see Sect. 3.2).

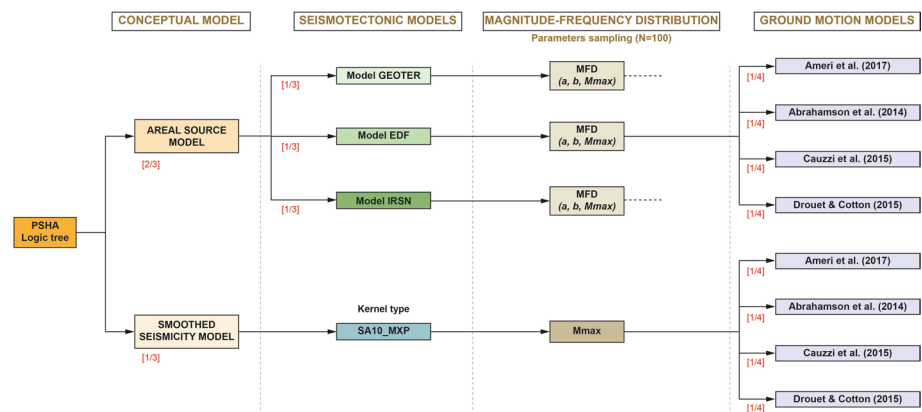
Figure 19 shows the logic-tree used for calculation.

The hazard is computed for 3 spectral periods PGA (100 Hz), 5 and 1 Hz. A grid of points with a mesh of 10 km is used covering the whole French metropolitan territory. Standard rock site conditions with  $v_{S30}=800$  m/s are considered. Finally, the minimum magnitude considered in PSHA calculations is  $M_w=4.5$ . To run the PSHA calculations we used one Geoter in-house software.

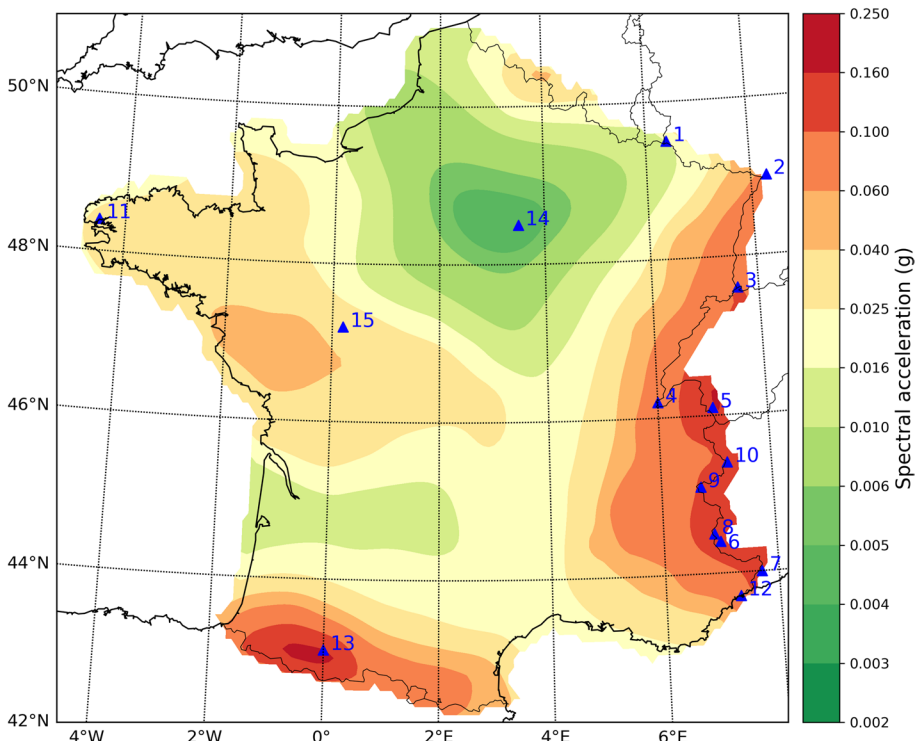
## 6 Results

Figure 20 presents the hazard map computed for the median PGA at 475 years return period. As expected, the highest hazard is obtained in the Alps and the Pyrenees. The Paris and Aquitan Basins as well as most of central France present a low hazard level. The Armorican region to the West is characterized by an intermediate hazard level. Maps of the 16th and 84th percentiles PGA at 475 years return period are shown in Figs. 21 and 22, respectively. The ratios between the two percentiles range between 1.7 and 4 with a median value around 2.4, which translates using the uncertainty measure defined by Douglas et al. (2014b)  $100 \times \log_{10}(PGA_{84}/PGA_{16})$  into 24, 61, and 39 as minimum, maximum and median values, respectively.

Depending on the location of the site of interest the models (SSC and GMC) have different impacts on the computed hazard. Figure 23 compares the ratios of the mean UHS at 475 years return period for the 16 main branches of the logic-tree (4 source models combined with 4 GMPEs) with respect to the mean UHS for the full weighted logic-tree for Brest and Nice (sites number 11 and 12 on Fig. 20, respectively). The color code allows the identification of the source model or the GMPEs used in the different branches. The figure shows that the uncertainty at Brest is controlled by the GMPE rather than by the source model while the opposite is observed for Nice where the source models have a stronger impact (e.g. the branches including the GTR source model lead to the higher hazard). This



**Fig. 19** Logic-tree used for PSHA calculation



**Fig. 20** Hazard map for median PGA at 475 years return period (10% probability of exceedance within 50 years). Blue triangles denote points where comparison with PSHA results from other studies are performed

is consistent with the results of the comparison of the activity rates shown in Fig. 14 for the same sites.

Hazard curves for the sites Brest and Nice are shown in Fig. 24 for PGA (0.01 s). In addition to the epistemic uncertainties related to the different logic-tree branches for the SSC and GMC model, the sampling of the seismic activity parameters ( $a$ ,  $b$ , and  $M_{max}$ ) contribute to the uncertainty.

## 7 Comparison with PSHA from neighbouring countries

The PSHA results obtained are compared with results from hazard models build independently for neighboring countries (Germany: Grünthal et al. 2018; Switzerland: Wiemer et al. 2016; Italy: Gruppo di Lavoro MPS, 2004) as well as with the results of the ESHM13 developed within the SHARE project (Woessner et al. 2015) and finally with the result of the hazard model for France developed in 2002 (MEDD2002).

We selected 10 points along the borders between France and neighboring countries as well as 5 additional points within the French territory at locations characterized by different hazard levels from low to high (Fig. 20). The median PGA values at 475 years return period predicted by the different hazard models are given in Table 8. Ratio of

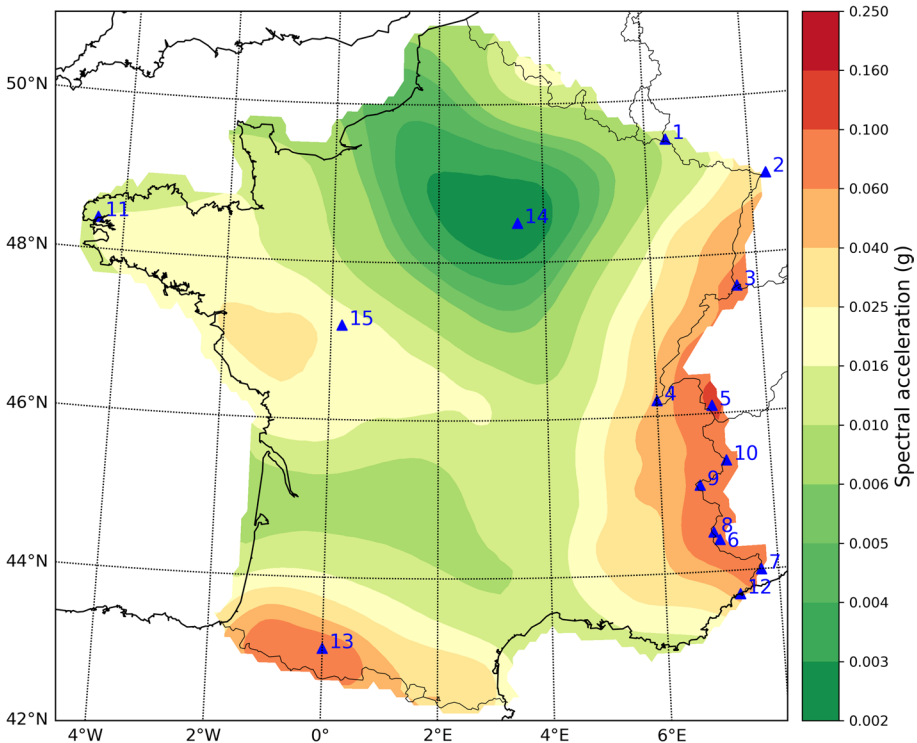


**Fig. 21** Hazard map for 16th percentile PGA at 475 years return period (10% probability of exceedance within 50 years). Blue triangles denote points where comparison with PSHA results from other studies are performed

the median PGA with respect to the results of the present study is also indicated (numbers in bracket). Note that standard rock conditions are considered in all models, with  $v_{S30}=800$  m/s, except the Swiss model which used  $v_{S30}=1150$  m/s.

The comparison shows a fair agreement between the recent PSHA studies for Germany, Switzerland, Italy and our results. The slight tendency to lower hazard predicted by the Swiss model may be linked with the different soil conditions considered ( $v_{S30}=1150$  m/s compared to 800 m/s in the other studies). The results from the ESHM13 model predict a higher hazard for all the considered sites; for 4 out of the 15 sites the ratio between the PGA predicted by ESHM13 and our model are larger than 2. Roughly speaking the median ESHM13 results correspond to the 84th percentile of the present study. Regarding the MEDD2002 model, it also predicts high hazard values; 8 out of the 15 sites present a PGA ratio above 2. This ratio reaches about 12 for the site in the middle of the Parisian Basin, the region with the lowest hazard level in France. These results are consistent with what already observed by Martin et al. (2017) for southeastern France.

Table 9 presents the results of the comparison between our results and those from the MEDD2002 model for 100 years return period. Again, the present study leads to lower hazard than the MEDD2002 study and the difference is larger at 100 years return period compared to 475 years return period.

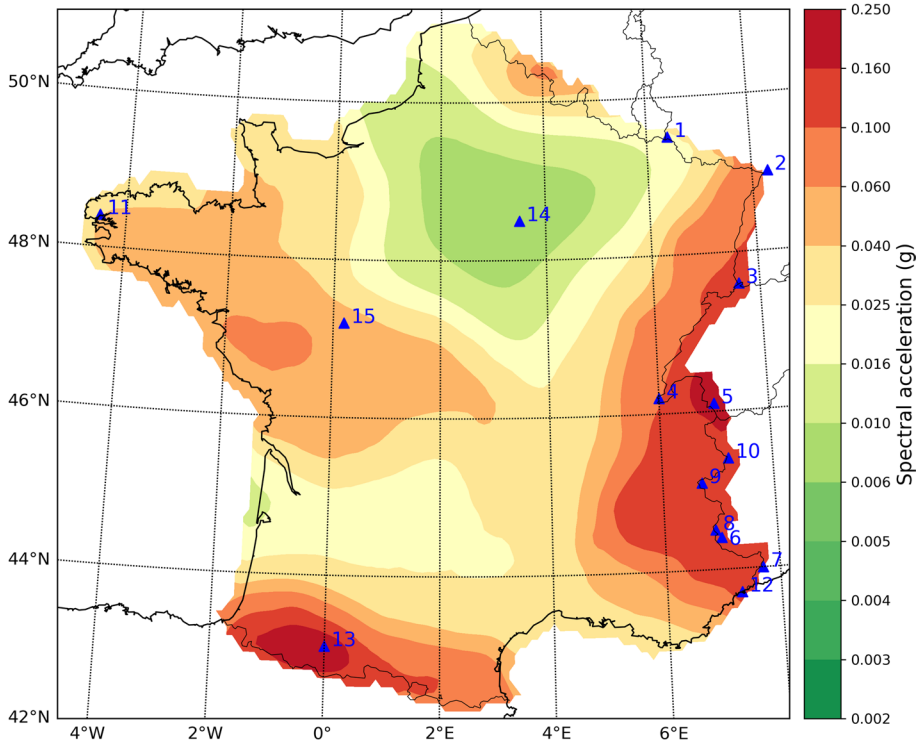


**Fig. 22** Hazard map for 84th percentile PGA at 475 years return period (10% probability of exceedance within 50 years). Blue triangles denote points where comparison with PSHA results from other studies are performed

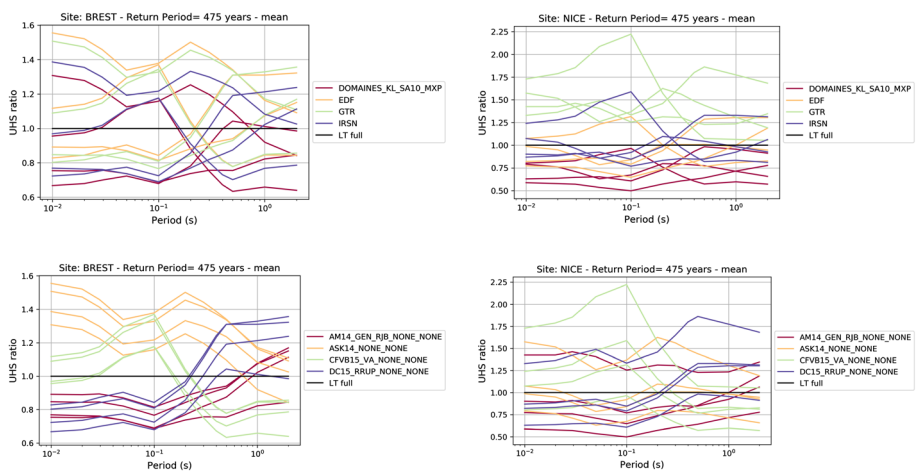


**Fig. 23** Ratios of the mean UHS at 475 years return period corresponding to the 16 main branches of the logic-tree (4 source models and 4 GMPEs) with respect to the mean UHS computed from the full weighted logic-tree. Two sites are compared Brest (left) and Nice (right). The same data are plotted on the upper and lower panels but the color code highlights source models (top) or GMPEs (bottom)

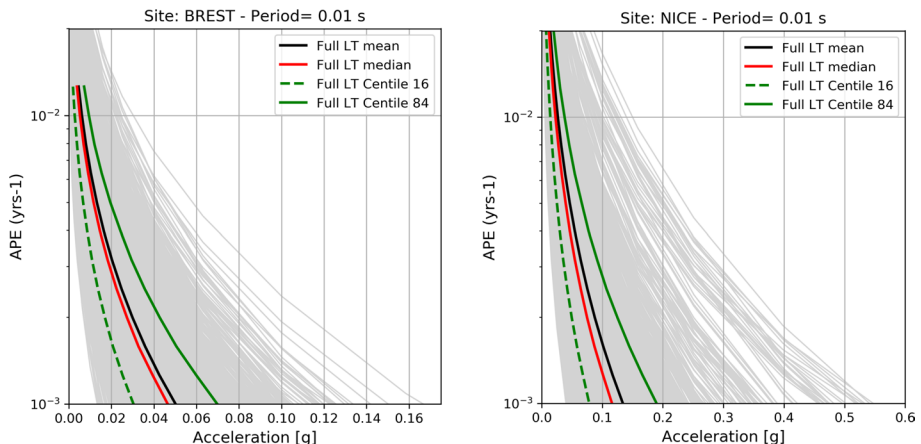


**Fig. 24** Hazard curves (Annual Probability of Exceedance APE versus acceleration) for PGA (0.01 s) for site Brest (left) and Nice (right). Mean, median and 16th and 84th percentiles are shown (black, red, dashed green and solid green curves, respectively), as well as all the hazard curves corresponding to all the branches of the logic-tree (grey curves)

In order to have a better understanding of how the PSHA studies compare, other spectral periods should be included, and uncertainties should also be compared but this is out of the scope of the present study.

The high hazard values predicted by the MEDD2002 model can largely be explained by the magnitude conversion scheme used at the time basically assuming  $M_S = M_L$ , and the GMPEs used which overestimate ground motion for moderate events (Bard et al. 2007).

## 8 Discussion

In the present study, we developed a hazard model for metropolitan France with the aim of producing a seismic hazard map for 475 years return period. The hazard model is the result of about 15 years of research and development since the first probabilistic hazard map for France. In particular, outcomes of the SIGMA project are included in the model (earthquake catalogue, maximum magnitude based on a Bayesian approach, GMPEs).

During the study, a number of limitations requiring further attention have been identified and will be addressed in future development of the model. The earthquake catalogue, mainly based on the FCAT-17 catalogue (Manchuel et al. 2017) lacks event-specific location uncertainty, which is used to assess the uncertainty on the seismic activity rates by generating synthetic catalogues. Moreover, for the purpose of improving the PSHA for the borders area, the consistency of FCAT-17 with catalogues from neighboring countries should be further and more systematically assessed.

In addition, the comparison of direct moment magnitude measures with the conversion scheme used to convert local magnitudes computed by LDG in France to moment magnitude indicates a discrepancy for local magnitudes below 4.0–4.5. The analysis of the observed seismic activity rates indicated a kink in the Gutenberg–Richter (GR) models in the same range of magnitude leading to different slopes of the GR model

**Table 8** Median PGA for 475 years return period predicted by different hazard models for 15 points of comparison. Numbers in brackets indicate the ratio with respect to the results from the present study

Site	Latitude (°N)	Longitude (°E)	Median PGA (g)	This study France $V_{S30}=800$ m/s	Grünthal et al. (2018) Germany $V_{S30}=800$ m/s	SUlhaz2015 ETH Switzerland $V_{S30}=1150$ m/s	Gruppo di Lavoro MPS (2004) Italy $V_{S30}=800$ m/s	ESHM13 Euro- Mediterranean region $V_{S30}=800$ m/s	MEDD2002 France $V_{S30}=800$ m/s
1	6.4	49.5	0.015	0.012 (0.8)	—	—	—	0.026 (1.8)	0.054 (3.6)
2	8.3	49.0	0.057	0.062 (1.1)	—	—	—	0.144 (2.5)	0.139 (2.4)
3	7.6	47.6	0.090	0.103 (1.1)	0.087 (1.0)	—	—	0.254 (2.8)	0.176 (2.0)
4	6.0	46.2	0.067	—	0.044 (0.7)	—	—	0.098 (1.5)	0.163 (2.4)
5	7.0	46.1	0.148	—	0.106 (0.7)	—	—	0.184 (1.2)	0.182 (1.2)
6	7.0	44.4	0.113	—	—	—	0.124 (1.1)	0.186 (1.7)	0.193 (1.7)
7	7.7	44.1	0.103	—	—	—	0.145 (1.4)	0.172 (1.7)	0.184 (1.8)
8	6.9	44.5	0.112	—	—	—	0.116 (1.0)	0.158 (1.4)	0.192 (1.7)
9	6.7	45.1	0.099	—	—	—	0.105 (1.1)	0.120 (1.2)	0.174 (1.8)
10	7.2	45.4	0.100	—	—	—	0.125 (1.2)	0.128 (1.3)	0.168 (1.7)
11	-4.5	48.4	0.026	—	—	—	—	0.039 (1.5)	0.093 (3.6)
12	7.3	43.7	0.073	—	—	—	—	0.161 (2.2)	0.151 (2.1)
13	0.0	43.1	0.154	—	—	—	—	0.295 (1.9)	0.226 (1.5)
14	3.5	48.5	0.004	—	—	—	—	0.013 (3.3)	0.046 (11.7)
15	0.2	47.2	0.032	—	—	—	—	0.050 (1.6)	0.112 (3.5)

**Table 9** Median PGA for 100 years return period predicted by this study and the MEDD2002 model for 15 points of comparison. Numbers in bracket indicate the ratio with respect to the results from the present study

Site	Median PGA (g)	
	This study France vs30 = 800 m/s	MEDD2002 France vs30 = 800 m/s
1	0.006	0.031 (5.2)
2	0.017	0.081 (4.8)
3	0.031	0.108 (3.5)
4	0.025	0.099 (4)
5	0.054	0.107 (2)
6	0.037	0.12 (3.3)
7	0.033	0.112 (3.4)
8	0.037	0.121 (3.3)
9	0.034	0.106 (3.1)
10	0.036	0.105 (2.9)
11	0.005	0.052 (10.3)
12	0.023	0.088 (3.8)
13	0.047	0.139 (3)
14	–	0.023 (–)
15	0.009	0.065 (7.3)

above and below this kink. This feature has already been observed by Beauval and Scotti (2003) and still needs to be resolved.

Regarding the estimation of seismic activity rates, further analysis on the impact of the completeness uncertainty and declustering scheme may also help to improve the hazard model. Moreover, in the present study, no correction on the activity rates has been applied. However, the EPRI (2012) shows that the propagation of uncertainty on the magnitude may lead to biased activity rates. In the meantime, the conversions from intensity or other magnitude scale to the target magnitude scale may also introduce counter-balancing bias. A careful review of the earthquake catalogue tracking the original measure of earthquake size together with its uncertainty and of the conversion schemes is needed to further investigate those effects.

Comparison of our results with recent PSHA studies for Germany, Switzerland and Italy show a fair agreement in terms of median PGA at 475 years return period. Compared with the ESHM13 and MEDD2002 PSHA results, our study leads to lower hazard at 475 years return period. In addition, the difference with MEDD2002 is higher for shorter return period (100 years).

Tasan et al. (2014) performed a testing of PSHA results against recorded accelerometric data in France. Their results showed that the MEDD2002 predictions were higher than the observations for 100 years return period while at longer return periods the tests were not conclusive due to limited amount of data. PSHA testing for larger hazard levels may be done using intensity data. Rey et al. (2018) performed such a comparison with the ESHM13 hazard model. These authors found that for half of the sites considered, the ESHM13 predictions are consistent with observations and lower for the other sites. Additional analyses in that direction are ongoing to further test the hazard model developed in the present study but are out of the scope of the present paper.

In addition to testing the PSHA results, testing may be performed at different steps (e.g. catalogues, ground-motion models). Beauval et al. (2012) tested several GMPEs against recorded accelerometric data in France. However, the GMPEs used in that study are now outdated and have not been used in the present paper. Initiatives are ongoing to build a comprehensive database of processed accelerometric records of events with magnitude greater than about 3 recorded on the French metropolitan territory (Traversa et al. 2018). Using this database to test the GMPEs selected in the Ground-Motion Model is planned in the future.

**Acknowledgements** The study has been funded by EDF. The authors would like to warmly thank Christophe Durouchoux, Nicolas Humbert, Emmanuel Viallet, Christophe Martin, Pierre Labb  , and Paola Traversa for fruitful discussions during meetings held all along the study. IRSN is also thanked for providing the IRSN area source model. The two anonymous reviewers and the Editor are also warmly thanked for their constructive comments which helped to improve the manuscript.

## References

- Abrahamson N, Silva WJ (2008) Summary of the Abrahamson & Silva NGA ground-motion relations. *Earthq Spectra* 24:67–97
- Abrahamson N, Silva WJ, Kamai R (2014) Summary of the ASK14 ground-motion relation for active crustal regions. *Earthq Spectra* 30(3):1025–1055
- Akkar S, Bommer JJ (2010) Empirical equations for the prediction of PGA, PGV and spectral accelerations in Europe, the Mediterranean region and the Middle East. *Seismol Res Lett* 81(2):195–206
- Akkar S, Sandikkaya MA, Senyurt M, Azari Sisi A, Ay B  , Traversa P, Douglas J, Cotton F, Luzi L, Hernandez B, Godey S (2014) Reference database for seismic ground-motion in Europe (RESORCE). *Bull Earthq Eng* 12(1):311–339
- Ameri G (2014) Empirical ground motion model adapted to the French context. Deliverable SIGMA: SIGMA-2014-D2-131
- Ameri G, Baumont D, Gomes C, Le Dortz K, Le Goff B, Martin C, Secanell R (2015) On the choice of maximum earthquake magnitude for seismic hazard assessment in metropolitan France—insight from the Bayesian approach. In: 9  me Colloque National AFPS 2015, 30 novembre-2 d  cembre 2015, IFSTTAR
- Ameri G, Drouet S, Traversa P, Bindu D, Cotton F (2017) Toward an empirical ground motion prediction equation for France: accounting for regional differences in the source stress parameter. *Bull Earthq Eng*. <https://doi.org/10.1007/s10518-017-0171-1>
- Autran A., Bles J-L, Combes P, Cushing M, Dominique P, Durouchoux C, Gariel J-C, Goula X, Mohammedioun B, Terrier M (1998) Probabilistic seismic hazard assessment in France. In: Part one: seismotectonic zonation—11th European conference on earthquake engineering, Balkema, Rotterdam
- Baize S, Cushing EM, Lemeille F, Jomard H (2013) Updated seismotectonic zoning scheme of Metropolitan France, with reference to geologic and seismotectonic data. *Bull Soc G  ol France* 184(3):225–259
- Bakun WH, McGarr A (2002) Differences in attenuation among the stable continental regions. *Geophys Res Lett* 29(23):2121. <https://doi.org/10.1029/2002GL015457>
- Bard P-Y, Hernandez B, Jalil W, Labb   P, Mouroux P, Sollogoub P, Viallet E (2007) AFPS French zoning group report. <https://doi.org/10.13140/RG.2.2.10423.01447>
- Baumont D, Manchuel K, Traversa P, Durouchoux C, Nayman E, Ameri G (2018) Intensity predictive attenuation models calibrated in Mw for metropolitan France. *Bull Earthq Eng* 16(6):2285–2310
- Beauval C, Scotti O (2003) Mapping b-values in France using two different magnitude ranges: possible non power-law behavior. *Geophys Res Lett*. <https://doi.org/10.1029/2003GL017576>
- Beauval C, Tasan H, Laurendeau A, Delavaud E, Cotton F, Gu  guen P, Kuehn N (2012) On the testing of ground-motion prediction equations against small-magnitude data. *Bull Seismol Soc Am* 102(5):1994–2007
- Berge-Thierry C, Cushing E, Scotti O, Bonilla F (2004) Determination of the seismic input in France for the nuclear power plants safety. Regulatory context, hypothesis and uncertainties treatment. In: Proceedings of the CSNI workshop on seismic input motions, incorporating recent geological studies, Tsukuba, Japan, 15–17 November

- Bles JL, Bour M, Dominique P, Godefroy P, Martin C, Terrier M (1998) Zonage sismique de la France métropolitaine pour l'application des règles parasismiques aux installations classées. BRGM, Document n° 279, 56 p., 8 fig., 5 tabl
- Bozorgnia et al (2014) NGA-West2 research project. *Earthq Spectra* 30(3):973–987
- Burkhard M, Grünthal G (2009) Seismic source zone characterization for the seismic hazard assessment project PEGASOS by the Expert Group 2 (EG1b). *Swiss J Geosci* 102:149–188. <https://doi.org/10.1007/s00015-009-1307-3>
- Camelbeeck T, Alexandre P, Vanneste K, Meghraoui M (2000) Long term seismicity in regions of present day low seismic activity: the example of western Europe. *Soil Dyn Earthq Eng* 20:405–414
- Cara et al (2015) SI-Hex: a new catalogue of instrumental seismicity for metropolitan France. *Bull Soc Géol France* 186(1):3–19
- Cara M, Denieul M, Sèbe O, Delouis B, Cansi Y, Schlupp A (2017) Magnitude Mw in metropolitan France. *J Seismol* 21:551–565. <https://doi.org/10.1007/s10950-016-9617-1>
- Cauzzi C, Faccioli E (2008) Broadband (0.05 to 20 s) prediction of displacement response spectra based on worldwide digital records. *J Seismol* 12(4):453–475
- Cauzzi C, Faccioli E, Vanini M, Bianchini A (2015) Updated predictive equations for broadband (0.01 to 10 s) horizontal response spectra and peak ground motions, based on a global dataset of digital acceleration records. *Bull Earthq Eng* 13(6):1587–1612
- Delavaud E, Cotton F, Akkar S, Scherbaum F, Danciu L et al (2012) Toward a ground-motion logic tree for probabilistic seismic hazard assessment in Europe. *J Seismol* 16(3):451–473
- Delvaux D (1993) The TENSOR program for paleostress reconstruction: examples from the east African and the Baikal rift zones. In: *Terra Abstracts. Abstract supplement No. 1 to Terra Nova*, 5, 216
- Delvaux D, Sperner B (2003) New aspects of tectonic stress inversion with reference to the TENSOR program. In: Nieuland DA (ed) *New insights into structural interpretation and modelling*, vol 212. Geological Society, London, Special Publications, pp 75–100
- Douglas J, Akkar S, Ameri G, Bard P-Y, Bindi D et al (2014a) Comparisons among the five ground-motion models developed using RESORCE for the prediction of response spectral accelerations due to earthquakes in Europe and the Middle East. *Bull Earthq Eng* 12(1):341–358
- Douglas J, Ulrich T, Bertil D, Rey J (2014b) Comparison of the ranges of uncertainty captured in different seismic-hazard studies. *Seismol Res Lett* 85(5):977–985
- Drouet S, Cotton F (2015) Regional stochastic GMPEs in low-seismicity areas: scaling and aleatory variability analysis—application to the French Alps. *Bull Seismol Soc Am* 105(4):1883–1902
- Drouet S (2017) Erratum to regional stochastic GMPEs in low-seismicity areas: scaling and aleatory variability analysis—application to the French Alps. *Bull Seismol Soc Am* 107(1):501–503
- EPRI (2012) Technical report: Central and Eastern United States Seismic Source Characterization for Nuclear Facilities. EPRI, Palo Alto, CA, U.S. DOE, and U.S. NRC: 2012
- Faccioli E, Paolucci R, Vanini M (2015) Evaluation of probabilistic site-specific seismic-hazard methods and associated uncertainties, with applications in the Po Plain. *Bull Seismol Soc Am*, Northern Italy. <https://doi.org/10.1785/0120150051>
- Gardner JK, Knopoff L (1974) Is the sequence of earthquakes in Southern California, with aftershocks removed, Poissonian? *Bull Seismol Soc Am* 64(5):1363–1367
- Grellet B, Combes P, Granier T, Philip H (1993) Sismotectonique de la France métropolitaine dans son cadre géologique et géophysique avec atlas de 23 cartes au 1/4.000.000ème et 1 carte au 1/1.000.000ème. ISPNO, Mémoire de la Société Géologique de France, 2 Vol., n° 164, 76 p., 19 Pl., 1 carte
- Grünthal G, Stromeier D, Bosse C, Cotton F, Bindi D (2018) The probabilistic seismic hazard assessment of Germany—version 2016, considering the range of epistemic uncertainties and aleatory variability. *Bull Earthq Eng* 16:4339–4395
- Gruppo di Lavoro MPS (2004). Redazione della mappa di pericolosità sismica prevista dall'Ordinanza PCM 3274 del 20 marzo 2003. Rapporto Conclusivo per il Dipartimento della Protezione Civile, INGV, Milano-Roma, aprile 2004, 65 pp. + 5 appendici
- Hakimhashemi AH, Grünthal G (2012) A statistical method for estimating catalog completeness applicable to long-term nonstationary seismicity data. *Bull Seismol Am* 102(6):2530–2546
- Heidbach O, Tingay M, Barth A, Reinecker J, Kurfeß D, Müller B (2009) Global crustal stress pattern based on the World Stress Map database release 2008. *Tectonophysics*. <https://doi.org/10.1016/j.tecto.2009.1007.1023>
- Helmstetter A, Werner MJ (2012) Adaptive spatiotemporal smoothing of seismicity for long-term earthquake forecasts in California. *Bull Seismol Soc Am* 102(6):2518–2529
- Johnston AC, Kanter LR, Coppersmith KJ, Cornell CA (1994) The earthquakes of stable continental regions. Tech. Rep. Electric Power Research Institute (EPRI), Palo Alto, California

- Le Dortz K, Combes P, Carbon D (2019) An alternative seismotectonic zonation for probabilistic and deterministic seismic hazard assessment for Metropolitan France, 10ème Colloque National AFPS
- Manchuel K, Traversa P, Baumont DM, Cara M, Nayman E, Durouchoux C (2017) The French seismic CATalogue (FCAT-17). Bull Earthquake Eng. <https://doi.org/10.1007/s10518-017-0236-1>
- Marin S, Avouac J-P, Nicolas M, Schlupp A (2004) A probabilistic approach to seismic hazard in metropolitan France. Bull Seismol Soc Am 94(6):2137–2163. ISSN 0037-1106
- Martelet G, Pajot G, Debeglia N (2009) Nouvelle carte gravimétrique de la France. RCGF09—Réseau et Carte Gravimétrique de la France, 2009. Rapport BRGM/RP-57908-PR, 77 p. 26 fig., 2 ann
- Martin C, Secanell R, Combes C, Lignon G (2002) Preliminary probabilistic seismic hazard assessment of France. In: 12th European conference on earthquake engineering, Londres, 9–13 septembre
- Martin C, Ameri G, Baumont D, Carbon D, Senfaute G, Thiry JM, Faccioli E, Savy J (2017) Probabilistic seismic hazard assessment for South-Eastern France. Bull Earthq Eng 16(6):2477–2511. <https://doi.org/10.1007/s10518-017-0249-9>
- Papazachos BC, Scordilis EM, Panagiotopoulos DG, Papazachos CB, Karakasis GF (2004) Global relations between seismic fault parameters and moment magnitude of earthquakes. In: Proceeding of the 10th international congress, Thessaloniki, April, Bulletin of the Geological Society of Greece, vol 36, pp 1482–1489
- Pecker A, Faccioli E, Gurpinar A, Martin C, Renault P (2017) An overview of the SIGMA research project. Springer, Berlin. <https://doi.org/10.1007/978-3-319-58154-5>
- Petersen MD, Harmsen SC, Jaiswal KS, Rukstales KS, Luco N, Haller KM, Mueller CS, Shumway AM (2018) Seismic hazard, risk, and design for south America. Bull Seismol Soc Am 108(2):781–800
- Reasenberg EA (1985) Second-order moment of central California seismicity. J Geophys Res 90:5479–5495
- Rey J, Beauval C, Douglas J (2018) Do French macroseismic intensity observations agree with expectations from the European Seismic Hazard Model 2013? J Seismol 22:589–604
- RFS 2001-01 (2001) French safety rule, published by the French Nuclear Safety Authority. <https://www ASN.fr/Reglementer/Regles-fondamentales-de-surete/RFS-relatives-aux-REP/RFS-2001-1-RFS-I.1.c.-du-31-05-2001>
- Scherbaum F, Kuehn N, Ohrnberger M, Koehler A (2010) Exploring the proximity of ground-motion models using high-dimensional visualization techniques. Earthq Spectra 26(4):1117–1138
- Senfaute G, Pecker A, Labbé P, Sidaner J-F, Berge-Thierry C, Rzepka J-P, Contri P (2015) Contribution of the SIGMA research program to analyses of uncertainties in seismic hazard assessment, 9ème Colloque National. AFPS, France, p 2015
- SISFRANCE [www.sisfrance.net](http://www.sisfrance.net)
- Tasan H, Beauval C, Helmstetter A, Sandikkaya A, Guéguen P (2014) Testing probabilistic seismic hazard estimates against accelerometric data in two countries: France and Turkey. Geophys J Int 198:1554–1571
- Tinti S, Mulargia F (1985) Effects of magnitude uncertainties on estimating the parameters in the Gutenberg–Richter frequency-magnitude law. Bull Seismol Soc Am 75(6):1681–1697
- Traversa P, Baumont DM, Manchuel K, Nayman E (2017) Exploration tree approach to estimate historical earthquakes Mw and depth, test cases from the French past seismicity. Bull Earthq Eng. <https://doi.org/10.1007/s10518-017-0178-7>
- Traversa P, Maufroy E, Hollender F, Foundotos L, Perron V, Drouet S, Shible H, Dauchy C, Herve F, Gueguen P (2018) RAP-RESIF ground motion dataset. Abstract n° ESC2018-S15–891, 36th General Assembly of the European Seismological Commission, 2–7 September 2018, Valletta, Malta
- Vanneste K, Verbeeck K (2001) Paleoseismological analysis of the Rurrand fault near Jülich Roer Valley graben, Germany: Coseismic or aseismic faulting history? Netherlands J Geosci Geol Mijnbouw 80(3–4):155–169
- Vanneste K, Camelbeeck T, Verbeeck K (2013) A model of composite seismic sources for the lower Rhine Graben. Northwest Europe. Bull Seismol Soc America 103(2A):984–1007. <https://doi.org/10.1785/0120120037>
- Weichert DH (1980) Estimation of the earthquake recurrence parameters for unequal observation periods for different magnitudes. Bull Seismol Soc Am 70:1337–1346
- Wells D, Coppersmith KJ (1994) New empirical relationships among magnitude, rupture length, rupture area & surface displacement. Bull Seismol Soc Am 84(4):974–1002
- Wesnousky SG (2008) Displacement and geometrical characteristics of earthquake surface ruptures: issues and implications for seismic-hazard analysis and the process of earthquake rupture. Bull Seismol Soc Am 98(4):1609–1632
- Wiemer S, Giardini D, Fäh D, Deichmann N, Sellami S (2009) Probabilistic seismic hazard assessment of Switzerland: best estimates and uncertainties. J Seismol 13:449–478

- Wiemer S, Danciu L, Edwards B, Marti M, Fäh D, Hiemer S, Wössner J, Cauzzi C, Kästli P, Kremer K (2016) Seismic hazard model 2015 for Switzerland (SUIhaz2015). Swiss Seismological Service (SED) at ETH Zurich
- Woessner et al (2015) The 2013 European Seismic hazard model: key components and results. *Bull Earthq Eng* 13(12):3553–3596
- Woo G (1996) Kernel estimation methods for seismic hazard area source modeling. *Bull Seismol Soc Am* 86(2):353–362
- Ziegler PA, Dézes P (2006) Crustal evolution of western and central Europe. *Geol Soc Lond Mem* 32:43–56. <https://doi.org/10.1144/GSL.MEM.2006.032.01.03>

**Publisher's Note** Springer Nature remains neutral with regard to jurisdictional claims in published maps and institutional affiliations.